FOR FURTHER TRAN

(14) PANA-RIPA-1

(6) RADIATION-INDUCED PARTICULATE
AGGLOMERATION FEASIBILITY STUDY.

(11) Apr 78   (12) 59 p.

(9) Rept. for 31 Mar 77 – 31 Mar 78
on Phase 1,

Submitted to

Harvard University
Harvard School of Public Health
Dept. of Environmental Health Engineering
665 Huntington Avenue
Boston, Massachusetts 02115
Project Officer: Melvin W. First
Purchase Order No. J35490

by

PANAMETRICS, INC.
221 Crescent Street
Waltham, Massachusetts 02154

Prepared by

(10) Bach Sellers and Frederick A. Hanser
Panametrics, Inc.

and

Lee W. Parker
Lee W. Parker, Inc.
252 Lexington Road
Concord, Massachusetts 01742

DDC
RECEIVED
JUN 29 1978
A

78 06 29 053
403 420

REPORT DOCUMENTATION PAGE		READ INSTRUCTIONS BEFORE COMPLETING FORM
1. REPORT NUMBER PANA-RIPA-1	2. GOVT ACCESSION NO.	3. RECIPIENT'S CATALOG NUMBER
4. TITLE (and Subtitle) Radiation Induced Particulate Agglomeration Feasibility Study		5. TYPE OF REPORT & PERIOD COVERED Phase I, 31 March 1977 to 31 March 1978
		6. PERFORMING ORG. REPORT NUMBER PANA-RIPA-1
7. AUTHOR(s) Bach Sellers, Frederick A. Hanser and Lee W. Parker		8. CONTRACT OR GRANT NUMBER(s) P.O. No. J93590
9. PERFORMING ORGANIZATION NAME AND ADDRESS Panametrics, Inc. 221 Crescent St. Waltham MA 02154		10. PROGRAM ELEMENT, PROJECT, TASK AREA & WORK UNIT NUMBERS
11. CONTROLLING OFFICE NAME AND ADDRESS Harvard School of Public Health Dept. of Environmental Health Engineering Boston MA 02115		12. REPORT DATE April 1978
		13. NUMBER OF PAGES 58
14. MONITORING AGENCY NAME & ADDRESS(If different from Controlling Office)		15. SECURITY CLASS. (of this report) Unclassified
		15a. DECLASSIFICATION/DOWNGRADING SCHEDULE

16. DISTRIBUTION STATEMENT (of this Report)

Approved for public release, distribution unlimited. Reproduction in whole or in part is permitted for any purpose of the United States Government.

17. DISTRIBUTION STATEMENT (of the abstract entered in Block 20, If different from Report)

18. SUPPLEMENTARY NOTES

This is a joint-authorship report between Panametrics, Inc. and Lee W. Parker, Inc. The work was carried out for the E.R.D.A. through P.O. No. J93590 with Harvard University.

19. KEY WORDS (Continue on reverse side if necessary and identify by block number)
Particle filtration
Radiation-induced charging
Radiation-induced agglomeration

20. ABSTRACT (Continue on reverse side if necessary and identify by block number)
The removal of aerosol particles from a gas by standard gas filtration techniques is more difficult for submicron particles than for larger particles. Filtration methods presently in use can achieve high efficiencies of submicron particle removal by use of high-efficiency HEPA filters. The system investigated is intended to agglomerate fine particles into larger sizes so that they are more easily captured by inexpensive low-efficiency prefilters used ahead of the more expensive HEPA filters.

78 06 29 053

The basic concept involves use of a beta radiation source to generate an intense volume of ionization. Application of an electric field to plates enclosing this volume then produces separate regions of positive and negative ions through which the particulate-containing air passes. After leaving this charging stage the oppositely-charged particulate distributions enter an agglomeration stage in which the polarity on the enclosing plates is reversed, so that particles of opposite sign are brought into close proximity, hence producing agglomeration and shifting the particle distribution toward larger sizes. With 20 kV on the plates, the charging times can be on the order of one second or less. The agglomeration of the small particles onto the large ones can occur in a few seconds, depending on the mass loading. This implies that particulate filtration can be enhanced by this technique.

TABLE OF CONTENTS

LIST OF ILLUSTRATIONS AND TABLES

1. INTRODUCTION

This report is concerned with results of the first part of a feasibility study of an improved air filtration system. It uses ionization-producing beta-ray isotope radiation, in conjunction with electric charging and acceleration, to cause fine particles to agglomerate, hence enhancing the subsequent collection process.

The removal of aerosol particles from a gas by any of the standard gas-cleaning techniques (filtration, scrubbing, or electrostatic precipitation) is known to be more difficult for submicron particles than for larger particles. Filtration methods presently in use can achieve high efficiencies of submicron particle removal, using high-efficiency HEPA filters. These filters are costly to build and replace. Moreover, frequent replacement as is necessary in some applications implies a large amount of system shutdown time. In the present state-of-the-art inexpensive low-efficiency prefilters are used ahead of the HEPA filters to capture the bulk of the aerosol mass residing in the larger particles. The finer particles not captured by the prefilters then pass into the HEPA filters. To the extent that the prefilters can be made more efficient in capturing fine particles, the lifetime of the HEPA filters can be prolonged, with a corresponding reduction in cost and shutdown time.

The system investigated is intended to agglomerate fine particles into larger sizes so that they are more easily captured by the prefilters.

The following sections give details of the filtration enhancement system and the key physical processes including ionization, particle-charging, and agglomeration. The physical parameters of the system are presented first; then the electrical and operational parameters are determined which are required for the system to demonstrate significant radiation-induced particulate agglomeration. A preliminary evaluation of the system feasibility is then given; the report concludes with recommendations relative to the further experimental and analytical work necessary to fabricate a model and to verify the predicted filtration-enhancement characteristics of the system.

1

2. THE FILTRATION ENHANCEMENT SYSTEM

2.1 Basic Description

The proposed system consists of a charging stage, followed by one or more agglomerating stages (see Fig.2.1). As illustrated, each stage is essentially a cylindrical tube. Within each tube the gas flows along isolated sections, of pie-shaped cross section, partitioned from one another by radial vanes (see Fig.2.2). Along the axis of the first tube, which is the charging stage, is an inner cylinder containing radio-active material (for example, ^{85}Kr gas). In this stage, the gas outside the inner tube is ionized by the radiation passing through the wall of the inner tube. DC voltages of alternating sign are applied to alternating partition vanes (Fig.2.2). These applied voltages cause the ions to con-centrate in separate unipolar regions. The gas containing the particles to be agglomerated flows through these unipolar regions by a flow-splitting geometry (Fig.2.2).

After the particles become charged in the charging stage, they pass into the first agglomerating stage. This stage has partitioning vanes identical to and aligned with those of the first stage, but the signs of the applied voltages are reversed. This forces oppositely-charged particles to move toward each other so that they would tend to agglomerate by collision. Particles failing to agglomerate in the first agglomerating stage pass into the next agglomerating stage where the vane voltages are again reversed. Hence, the particles, once charged, are accelerated toward oppositely-charged partners in successive passes in a sequence of agglomerating stages. The agglomerated particles can be separated from the unagglomerated particles by an appropriately designed (e. g. , impactor type) gas-flow system.

2

Air
containing
particulates to
be filtered

Cylindrical
Ionization-Induced
Charger Stage

Cylindrical
Reversed-Field
Agglomerator
Stage

Additional
Agglomerator and
Charger Stages as
Required

air containing
particulates with
distribution altered
toward larger sizes

Collection
(Filtration)
System
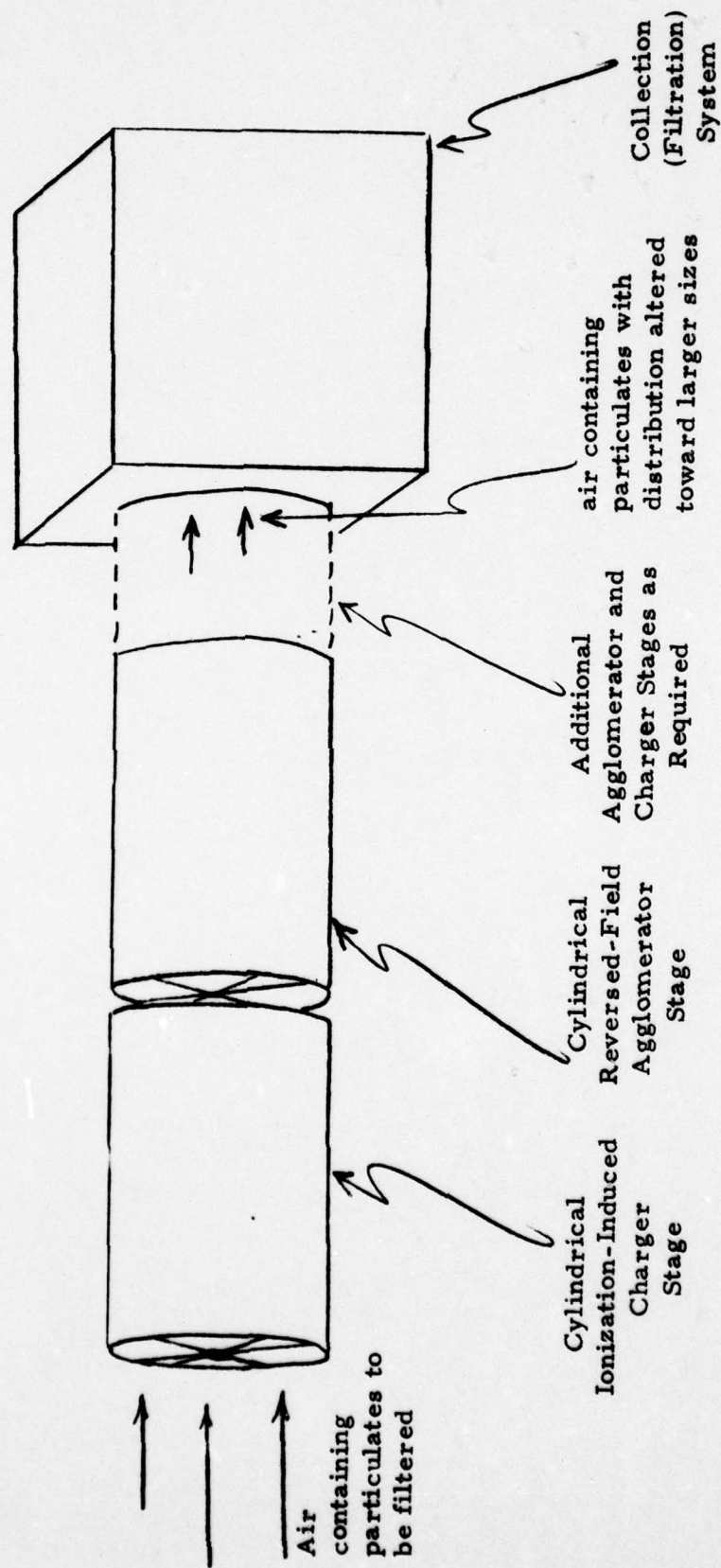
Fig. 2.1. Radiation-Induced Particulate Agglomeration System for Filtration Enhancement.

3

Ionization-Induced Charger,
showing ion distribution in
typical section

Typical diameter 50-100 cm

Radioactive gas in thin-walled
container to allow betas to
escape with minimum energy
loss

Vanes with DC voltage
of alternating sign

Collimator to limit
region of ionization
to center of pie-shaped
section

Ions are drawn toward
plate of opposite sign

Beta particles deposit
energy in ionization region,
producing charged ions

Agglomeration
region

After leaving Charger,
charged particulates
enter near vane of same
sign and move toward
particles of opposite
charge

Reversed-Field
Agglomerator

Fig. 2.2. Cross Sections of Charger and Agglomerator Showing Typical Pie-Shaped Section

4

2.2 Areas of Investigation

As discussed above, the basic concept involves use of a radiation source to produce separate regions of positive and negative ions through which the particulate-containing air passes (Fig. 2.2). After leaving the charging stage the oppositely-charged particulates enter an agglomeration stage (Fig. 2.1) in which the particles of opposite sign are brought into close proximity, hence producing agglomeration and shifting the particle distribution toward larger sizes. The result is that the average efficiency of the following collection system - be it scrubber, prefilter, etc. - is increased provided the average particle size is shifted past the well-known minimum (near 0.2-0.3 μm particle size) in the final stage collection system. The geometry for implementation of this concept as shown in Figs. 2.1 and 2.2 should be considered as illustrative only, not limiting. Other geometries (for example, rectangular) involving the same concept can be imagined.

There are five general areas requiring investigation:

1) Production of ionization by the radiation source.

2) Separation of ionization to produce a distribution having regions of predominantly positive and negative ions.

3) Charging of the particulates by the ions.

4) Agglomeration of the charged particles to shift distribution toward larger sizes.

5) Collection (filtration) of the altered particulate distribution.

As a first step in demonstrating feasibility of this concept it is necessary to show that sufficient ionization can be generated by realistic activity radioactive sources. The possibility of using ^{60}Co gamma radiation to generate ionization-producing electrons in a duct wall has been investigated by Heinsohn et al. (Ref. 2.1). Their intent was to produce charged particulates for purposes of electrostatic collection, a completely different objective from the present work. Furthermore, they did not separate the region of ionization production from those in

5

which the positive and negative ion distributions are maintained, as is done in Fig. 2.2. We believe that a beta source, which emits electrons directly, will prove to be of greater utility from the point-of-view of both handling and ionization production, than will a high energy gamma source. Krypton-85 appears to us to be of particular interest because of its availability, specific activity, and the range of its betas (up to ~200 cm). Hence the basic feasibility of producing ionization with this source is considered in some detail below. This is followed by a more general discussion of the other areas above, including the analytical methods applied to each.

In order to carry out the investigations of charging and agglomeration, it is desirable to consider particular particle size distributions. A number of typical particle size distributions encountered in nuclear materials handling facilities, and characterized as log-normal, are summarized in Table 2.1. This table is taken directly from a report by Lawrence Livermore Laboratory, where enhanced filtration mechanisms of a different type than that of interest here, are being investigated. It is seen that the particulates generally cover the range of about 0.2 to 30 microns, with median diameters of a few microns and standard deviations of 2-5.

Table 2.1

Typical particle distributions encountered in nuclear materials handling facilities. (From Ref. 2.2)

Facility	Process	Aerodynamic mass median diameter (μm)	Geometric std. dev. (σ_g)	Range (μm)	Principal constituents
LASL[6]	R&D	1.8	2.2	0.4 - 8.7	Pu
	R&D	2.3	3.5	0.2 - 28	Pu
	Fabrication	4.0	1.7	1.4 - 12	Pu
	Recovery	0.34	5.4	0.01 - 9.9	Pu
	Fabrication	2.7	2.4	0.5 - 16	Pu
Rocky Flats[7]	Recovery	0.9[a]	∿3	<0.3 - 13.7	Pu, HF, HNO$_3$
"Demonstration Plant"[b]	Grinding, 750°C	15.9	1.59	-	Pu U
"Industrial Plant"[b]	Grinding, 750°C	1.88	1.76	-	Pu U
"Demonstration, Industrial Plant"[b]	Grinding, 1750°C	2.30	1.65	-	Pu U
"Industrial Plant"[b]	Grinding, 1750°C	2.09	1.61	-	Pu U

[a] Count median diameter.

[b] G. Newton, Lovelace Foundation, private communication.

References 6) and 7) above are as follows:

6) H. J. Ettinger, J. C. Elder and M. Gonzales, Performance of Multiple HEPA Filters Against Plutonium Aerosols, LASL Report No. LA-5349-PR(1973).

7) R. W. Woodward, K. J. Grossaint, and J. L. McFeeters, Exhaust Filtration on Gloveboxes used for Aqueous Processing of Plutonium, 14th ERDA Air Cleaning Conference, Sun Valley, Idaho (1976).

3. CYLINDRICAL BETA SOURCE INDUCED IONIZATION DISTRIBUTION

In this section the ionization distribution results obtained from the ^{85}Kr beta source are presented and discussed first. This is followed by an analytical estimate of the ionization based on neglect of all scattering effects. This is known to be a poor approximation if the actual number distribution of the electrons is of interest. However, it is found here that reasonably good agreement with the experimental measurements can be obtained by this simple approach when only the ionization distribution is of interest.

3.1 Experimental Results

The basic configuration of the ^{85}Kr gaseous source used in this work is shown in the top portion of Fig. 2.2. The cylindrical beta source itself is surrounded by a collimator designed to limit the ionization region in the manner shown there. Fig. 3.1 is a reduction of a full-scale drawing of the source. The fabrication is completed by soldering a thin brass foil (~2 mil) over the entire outer surface to seal the assembly. The slots are the regions through which the betas enter the collimator apertures in Fig. 2.2; the solid portions of the source would be obscured by the collimator walls. This is necessary due to the scattering of the betas after passing through foil.

3.1.1 Measurement of Source Activity

The source was filled with gas to 0.10 atm. Since the specific activity of the gas was not precisely known, the resulting activity of the source was measured with the method outlined in Fig. 3.2.

2-1

see Detail A

End of tubing machined flat (both ends)

$11 \frac{15}{16}$

$\frac{3}{16}$

$\frac{1}{16}$

$\frac{3}{4}$ DIA

1 DIA

Detail A

60°

.350

Break Corners

.15°

Detail B

A   A

typ. $\frac{3}{16}$

$2\frac{3}{8}$ typ.

$\frac{3}{8}$ typ.

1.0 DIA

Inside Volume 114 cm³

Detail B

$\frac{1}{8}$

60° typ.

Fig. 3.1 Mechanical Design of the Gaseous Beta Source Housing.

Source Kr-85

Material : Brass tubing, seamless, tempered

Tol: ± $\frac{1}{32}$

Section A-A

9
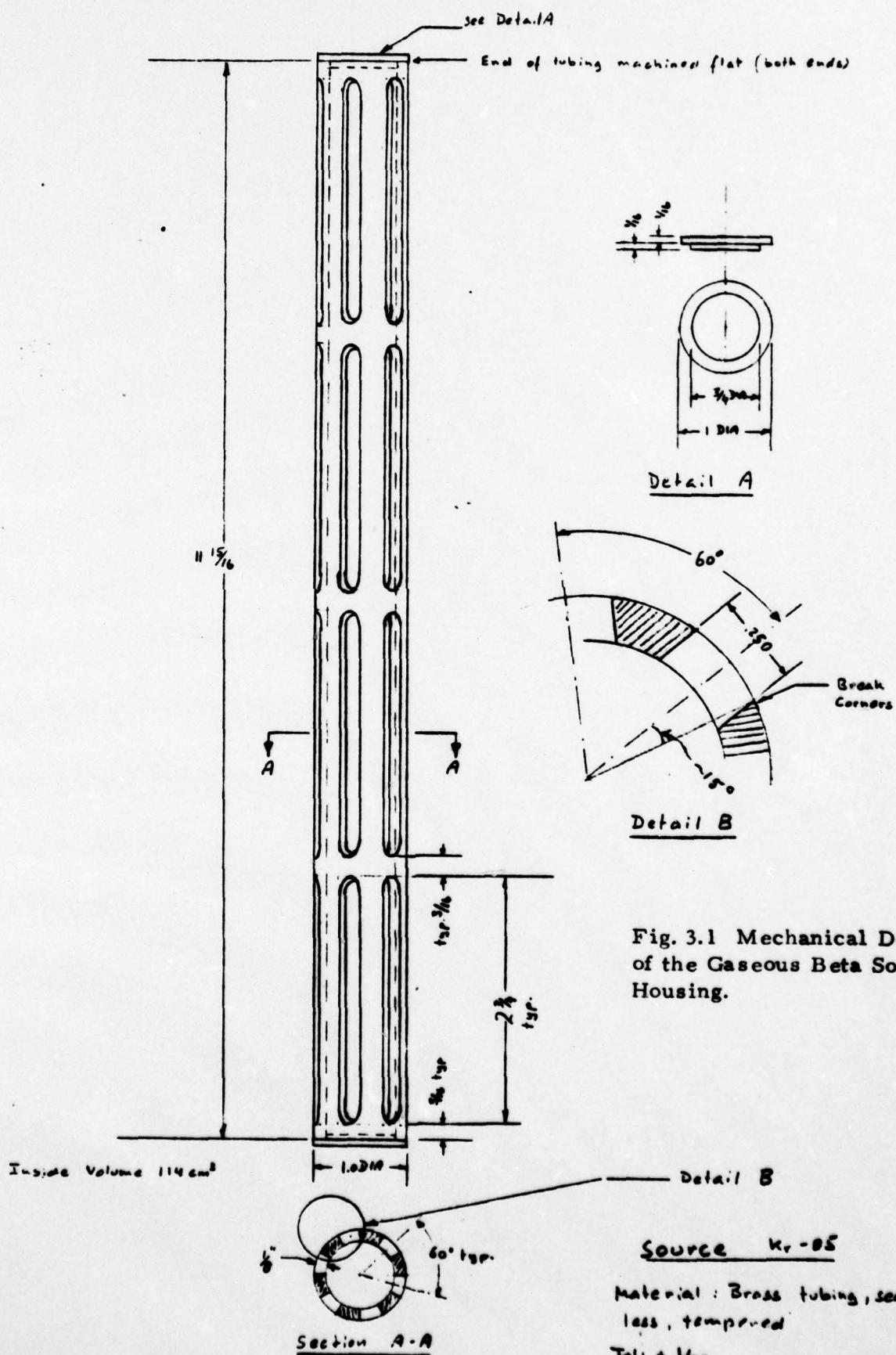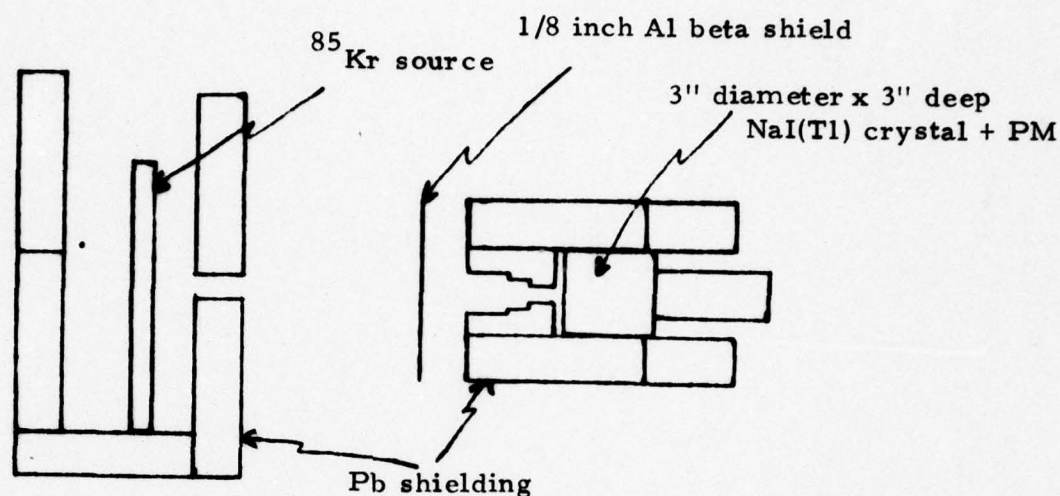
Fig. 3.2. Geometry for Measurement of ^{85}Kr Ionization Source Activity.

A well-shielded (2 inches of lead in all directions) 3 inch diameter x 3 inch deep NaI(Tl) crystal was used to detect the 0.514 MeV γ-ray emitted by ^{85}Kr in 0.41% of all decays. A central 1/2 inch diameter portion of the NaI(Tl) crystal was irradiated by a 3/4 inch section of the Kr source, all other portions of the source being shielded by 2 inches of lead. A piece of 1/8 inch aluminum was used to absorb the emitted beta particles and shield the NaI(Tl) crystal from this interference.

The total source activity can be written as

$$ S_a = \frac{C_p}{\epsilon_p F_o F_y F_s t_{Al} t_s} \tag{3.1} $$

where S_a is the source activity in disintegrations/sec, C_p is the measured NaI(Tl) count rate in the full energy peak (0.514 MeV) in cps, $\epsilon_p \simeq 0.80$ is the detection efficiency for the full energy peak, $F_o = 1.09 \times 10^{-4}$ is the fractional solid angle (of 4π) of the 1/2 inch diameter collimator, $F_y = 4.1 \times 10^{-3}$ is the

10

yield of 0.514 MeV γ-rays from ^{85}Kr, $F_s = 6.4 \times 10^{-2}$ is the fraction of the source viewed by the NaI(Tl) crystal, $t_{Al} = 0.93$ is the transmission of 1/8 inch Al for the 0.514 MeV γ-rays, and $t_s = 0.91$ is the transmission of the source walls for the 0.514 MeV γ-ray. The measurements gave $S_a = 1.04 \times 10^{10}$/sec, or $S_a = 0.28$ Ci of ^{85}Kr.

The method was checked by also measuring the activity of a 10μCi ^{137}Cs calibration source, detecting the 0.662 MeV γ-ray emitted in 85% of all decays ($F_y = 0.85$). Here $F_s = 1$, $t_s = 1$, $t_{Al} = 0.86$, $\epsilon_p \simeq 0.75$, and F_o is the same. The result gave 10.4μCi, and thus demonstrated the accuracy of the measurement.

The measurements show that the gas in the source is 1.7% ^{85}Kr by volume. Since the active volume of the source is 30.0 cm long, the specific activity of the source is 0.0093 Ci/cm.

3.1.2 Measurement of Ionization Distribution

The Kr ionization source was placed in the center of a four ft. long by 17-1/4 inch ID steel pipe (3/8 inch wall) and the radial ionization profile measured. This geometry was designed to simulate that of Fig. 2.2, except that the vanes and collimator are not present. The method is illustrated below.
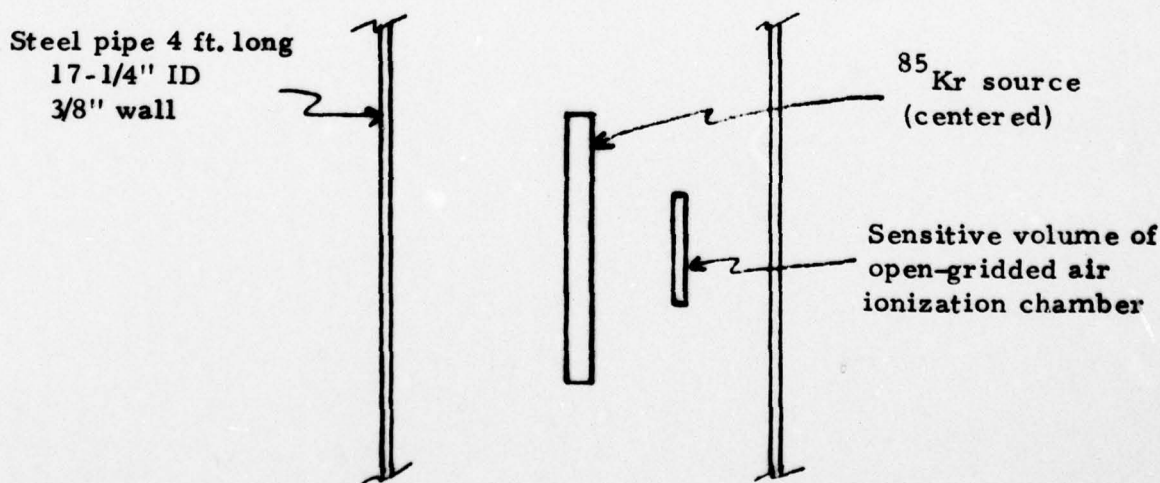

Steel pipe 4 ft. long
   17-1/4" ID
   3/8" wall

^{85}Kr source (centered)

Sensitive volume of open-gridded air ionization chamber

Fig. 3.3 Setup for Measuring ^{85}Kr Source-induced Ionization Distribution.

11

The ionization chamber is of the open-gridded air type, as described in Ref. 3.1. An outer shield mesh is held at ground potential, with an inner bias mesh 1.5 cm in diameter and 12.7 cm long defining the sensitive volume. The central wire is grounded through an electrometer to measure the ion current, while the inner mesh is held at ±100V through a 10 MΩ resistor. Tests of the ion chamber showed negligible current change for biases more than ±30V, and the sign of the bias voltage only affected the sign of the current measured, not its magnitude. The shield mesh voltage had a negligible effect on the measured current in the absence of significant air currents, and so was kept grounded. In the absence of ionizing radiation the leakage current was measured to be less than $\pm1\times10^{-14}$A for bias grid voltages of ±100V. The sensitive volume of the ion chamber is 22.0 cm^3, and it has been corrected for the volume of the central wire and bias grid support structure.

The ion chamber was scanned over center-to-center distances (radial, Kr source to ion chamber) of R = 5.5 to 17 cm, and the current measured. The current ranged from 4.50×10^{-10}A to 1.26×10^{-10}A. The ion production rates are

$$Q = I/(eV_i) \qquad (3.2)$$

where Q is in ion pairs/(cm^3-sec), I is the measured ion chamber current in A, $e = 1.60\times10^{-19}$ C is the electron charge, and $V_i = 22.0$ cm^3 is the ion chamber sensitive volume. The resulting Q profile, normalized to the source intensity, is shown in Fig. 3.4. The estimated uncertainty is $\pm20\%$.

At distances of 6-18 cm from the source, measurements were also made of the ionization distribution along a circumference. Very little such dependence was found, indicating that atmospheric scattering is a large effect, particularly in the absence of the collimators of Fig. 2.2.
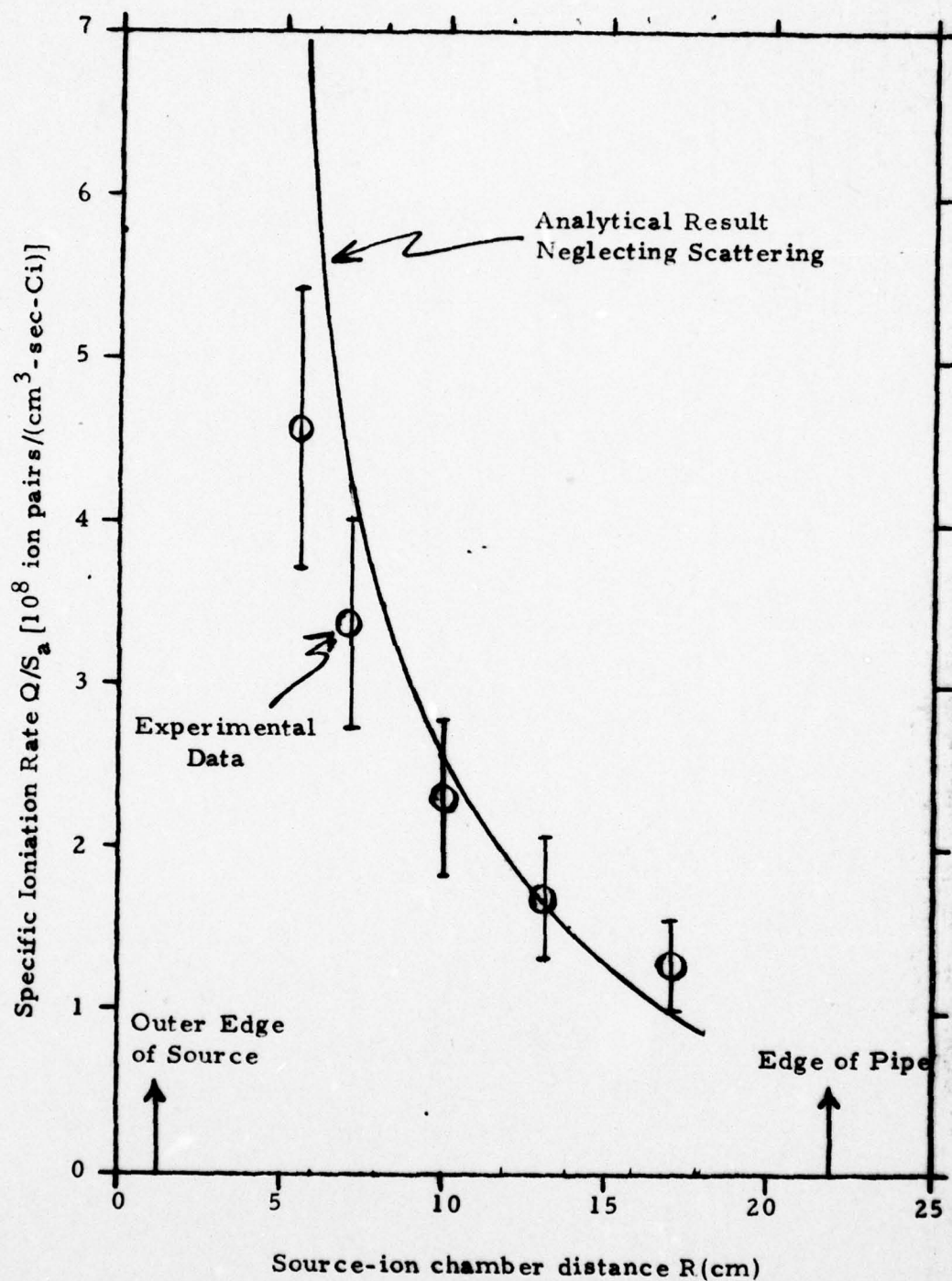
Fig. 3.4 Measured and Calculated Specific Ionization Distribution from ^{85}Kr Source.

13

3.2 Analytical Determination

Exact calculation of ionization distributions around sources such as that of Fig. 3.1 can only be made by Monte Carlo methods, in which scattering is included. Here we will make a calculation based on the approximation in which scattering is entirely neglected.

Consider the geometry shown in Fig. 3.5, which shows the source cross section and two points (a distance R from the source center) at which the calculation of ionization is to be made. Neglecting scattering, in each case only beta particles emitted from gas in the shaded areas can reach the points of interest. Note that, for the distance R shown (equivalent to 10 cm in actual scale) the effective area is about the same in each case. The measurements reported in 3.1 above found, in fact, that there was little dependence of the ionization rate on circumferential location. Hence, to do the calculation here we can replace the actual source by an "equivalent" source: an infinitely thin line source, covered by the foil, and having a source intensity equal to the average effective fraction of the gas in Fig. 3.5 times the actual source intensity. This fraction we find by graphical integration to be $f_e = 0.2116$ at $R = 10$ cm, and it is almost independent of R from 5 to 20 cm. The geometry for the calculation is given in Fig. 3.6.

The length of the source is L (cm), covered by a brass foil of thickness t_f (mil). The effective source intensity is

$$S_e = f_e S_a \text{ e/sec} \tag{3.3}$$

emitted isotropically into 4π steradians. The number of betas emitted per second from the element of length dX is the energy range dE (keV) is

$$j(E)dEdX = (S_e/L)\nu(E)dEdX \tag{3.4}$$

where $j(E)$e/(sec-keV-cm) is the emitted spectrum, normalized per unit length of the cylinder, and $\nu(E)$, which contains the energy dependence, is normalized to unity. From Ref. 3.2 it is seen that the spectrum is almost flat from 0 to 300 keV,

14

"Open Point". Located
diagonally opposite portion
of cylinder covered only
by foil.

"Obscured Point". Located
diagonally opposite a **solid**
portion of cylinder.

Source to Point
Distance **R**

Foil

Solid
portion
of
cylinder

Only radiation emitted from gas
in shaded regions can reach "Point"
in question without **scattering**
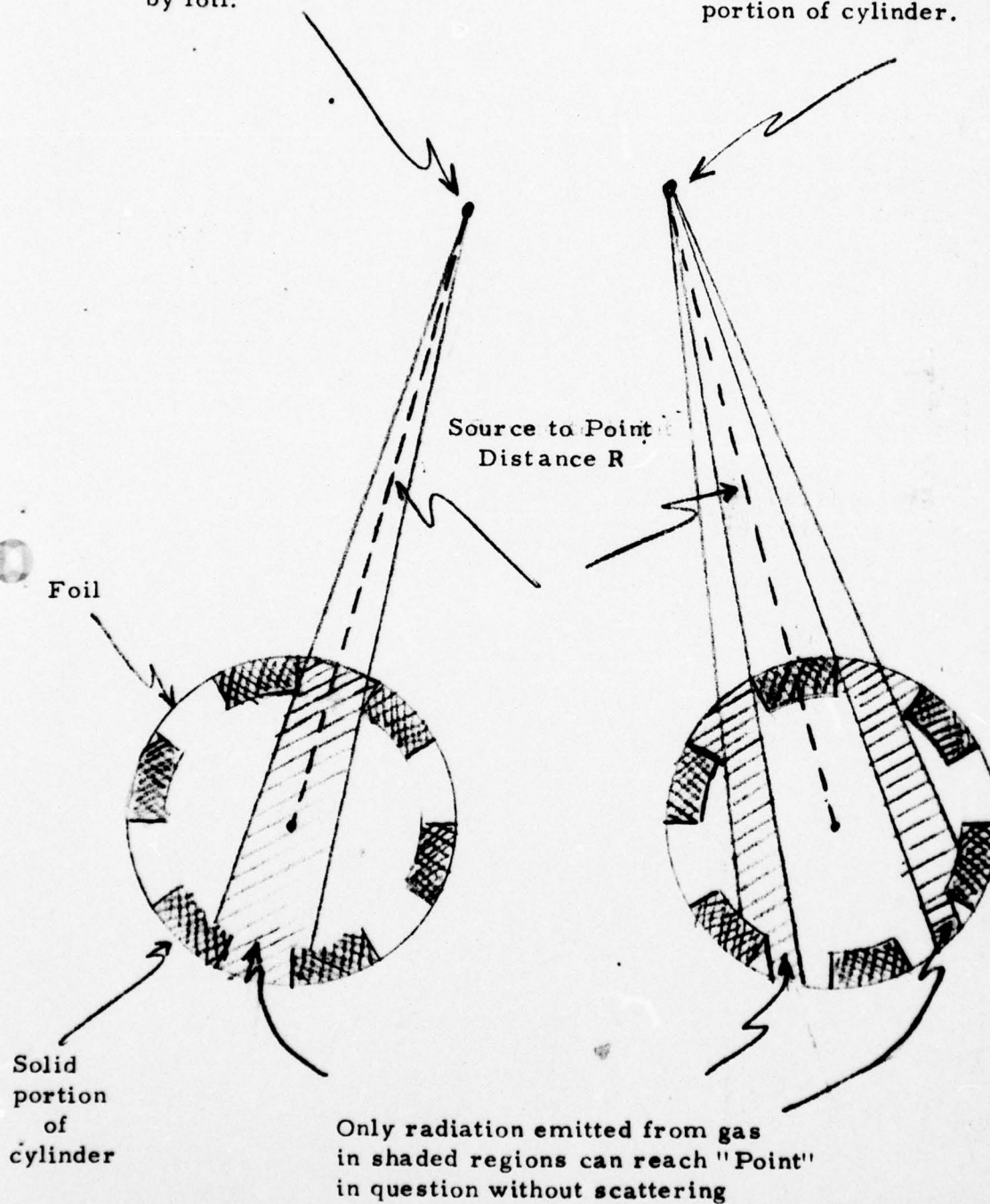
Fig. 3.5 Geometry for Calculation of Effective Gas Fraction.

15
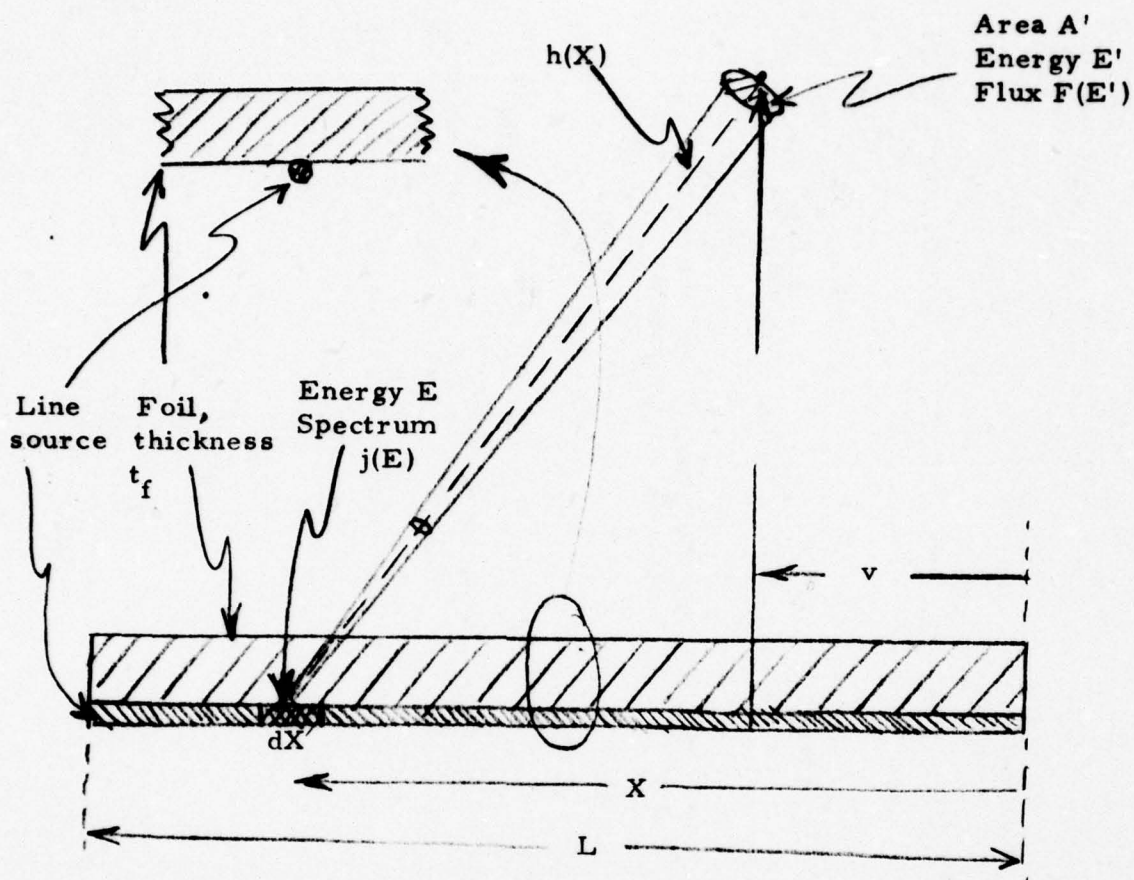
Fig. 3.6 Geometry for Analytical Determination of Ionization
Rate from Equivalent Source.

decreases linearly above the energy E_s = 300 keV and is zero at a maximum
energy E_m = 670 keV. Thus we set

$$\nu(E)dE = \nu_o dE \qquad\qquad 0 < E < E_s$$

$$\left. \begin{array}{l} = \nu_o dE(E_m - E)/(E_m - E_s) \quad E_s \leq E < E_m \\ \\ = 0 \qquad\qquad\qquad\quad E \geq E_m \end{array} \right\} \qquad (3.5)$$

and require that

$$1 = \int_0^{E_m} \nu(E)dE$$

which yields

$$\nu_o = 2/(E_s + E_m)\ \text{keV}^{-1} \tag{3.6}$$

completing the definition of $\nu(E)$ in (3.5) for use in (3.4).

The betas leave the element dX and pass through the foil and also through a length h(X) of air of density $\rho(\text{g/cm}^3) = 1.3 \times 10^{-3}\ \text{g/cm}^3$, where

$$h(X)^2 = R^2 + (X - \nu)^2\ \text{cm}^2 \tag{3.7}$$

As a result the energy is changed from E to E', and the flux of betas emitted by the element dX in the energy range dE' through the area A' at the point of interest is $F(E')e/(\text{cm}^2\text{-sec-keV-cm})$, where

$$F(E')dE'dX = \frac{j(E)dEdX}{4\pi h(X)^2} \tag{3.8}$$

The energy deposition rate $\mathcal{E}(\text{keV-cm}^{-3}\text{-sec}^{-1})$ at the point of interest, due to the entire beta spectrum and source length, is

$$\mathcal{E}(R, v) = \int_X \int_{E'} \rho S(E')F(E')dE'dX$$

$$= \frac{\rho f_e S_a}{4\pi L} \int_0^L \frac{dX}{h(X)^2} \int_0^{E_m} S(E')\nu(E)dE \tag{3.9}$$

The energy integral depends upon X and t_f through evaluation of the stopping power $S(E')(\text{keV-g}^{-1}\text{-cm}^2)$ at the energy E'(keV). For purposes of calculating the energy loss, the path length traversed is expressed in g/cm^2. Thus,

$$R(\text{g/cm}^2) = \rho R(\text{cm}) \tag{3.10}$$

17

Since the ratio of stopping power for copper (the foil is actually brass, but is essentially copper for present purposes) to that of air is almost independent of energy, we can equate the foil to an amount of air that would produce the same energy loss. Use of S(E) data from Ref. 3.3 for Cu and air yields

$$t_f(g/cm^2 \text{ air equiv.}) = .01745 \, t_f \text{ (mils Cu)} \qquad (3.11)$$

Hence, the path length $T(g/cm^2$ air) for a given R is

$$T = .01745 \, t_f(\text{mils}) + .0013 \, R(\text{cm}) \qquad (3.12)$$

and the path length equivalent to h(X) in g/cm^2 is then obtained from simple geometry and (3.12). (See (3.22) below).

The stopping power of air (Ref. 3.3) can be fitted by the following function with an error not exceeding about $\pm22\%$ from 10 to 900 keV,

$$S(E') = S_o(1 + E'/E_o)^{-m} \qquad (3.13)$$

where

$$S_o = 5.778 \times 10^5 \text{ keV-g}^{-1}\text{-cm}^2 \qquad (3.14)$$

$$m = .5478 \qquad (3.15)$$

$$E_o = .0135 \text{ keV} \qquad (3.16)$$

This stopping power expression is too low by about 40% at 1 keV, correct at 0.1 keV and too high below that. However, since the range of a 10 keV electron in air is only about 0.2 cm, inaccuracies in S(E) below 10 keV are unimportant for the present work. The total energy of each particle is deposited in the air surrounding the source no matter what S(E) expression is used; the present expression could lead to errors of 0.2 cm at most in the $\mathcal{E}(R, v)$ distribution. This error is certainly small compared to that due to neglect of scattering.

18

A significant advantage of the expression (3.13) is that it can be integrated to yield the distance $r(g/cm^2 air)$ required to change the energy from E to E',

$$r = \int_{E'}^{E} dE'/S(E') \tag{3.17}$$

$$= \frac{E_o}{S_o(m+1)} \left[(1 + E/E_o)^{m+1} - (1 + E'/E_o)^{m+1} \right] \tag{3.18}$$

The range-energy E_r is that value of E for which the residual energy $E'=0$ at r:

$$E_r(r) = E_o \left\{ [1 + S_o(m+1)r/E_o]^{1/(m+1)} - 1 \right\} \tag{3.19}$$

Solving (3.18) for E', and using it in (3.13) along with (3.19) shows that $S(E')$ can be written in terms of the initial energy E and the range energy E_r

$$S(E') = S_o f(E) \tag{3.20}$$

where

$$f(E) = \left[1 + (1 + E/E_o)^{m+1} - (1 + E_r/E_o)^{m+1} \right]^{-m/(m+1)} \tag{3.21}$$

E_r is evaluated for that path length r in g/cm^2 equivalent to the distance $h(X)$ in Fig. 3.6, i.e.

$$r(X, v) = T \sqrt{1 + (X-v)^2/R^2} \tag{3.22}$$

where T is given by (3.12).

The ion-electron pair production rate $Q(R, v)$ ion pairs-cm^{-3}-sec^{-1} is given by

$$Q(R, v) = \mathcal{E}(R, v)/I_i \tag{3.23}$$

where $I_i = .035$ keV/ion pair is the energy deposition in air necessary to create one ion-electron pair. By use of (3.9) and (3.20) this result can be written

19

$$Q(R, v)/S_a = \int_0^L (Q_x(R, v)/S_a)dX \qquad (3.24)$$

where

$$Q_x(R, v)/S_a = \frac{\rho f_e S_o}{4\pi I_i L h(X)^2} \int_{E_r}^{E_m} f(E)\nu(E)dE \qquad (3.25)$$

The lower limit on the energy integral has been replaced by E_r from (3.19) with r given by (3.22), since no particles with energy less than this can reach the point of interest. The result (3.24) is called the specific ionization rate. By converting S_a from e/sec to curies (Ci), where

$$1 \text{ Ci} = 3.7\text{x}10^{10} \text{e/sec} \qquad (3.26)$$

the units of Q/S_a are ion pairs/$(cm^3\text{-sec-Ci})$, and that of Q_x/S_a, the specific ionization rate per unit length, are ion pairs/$(cm^3\text{-sec-Ci-cm})$.

A FORTRAN program for computing the result (3.25) by double numerical integration is given in Table 3.1. The program input and typical output are given in Tables 3.2 and 3.3. The output tabulates (3.25) and (3.10) vs X and provides the final result (3.24) for that value of R following the table. More detailed results are given in Fig. 3.4, labelled "Analytical Result Neglecting Scattering." In general, it can be seen that the calculations agree rather well with the experimental data, thus reinforcing the general accuracy of both results.

As typical values for use in the charging and agglomeration work we choose $R = 10$ cm and $S_a = 500$ Ci, for which

$$Q \approx 10^{11} \text{ ion pairs}/(cm^3\text{-sec}) \qquad (3.27)$$

We note that this rate drops only by about a factor of 2 between 10 and 20 cm, so that a high rate is maintained throughout the volume of interest.

```
C           CYLION.FT:FIND ION DEPOSITION RATE FROM CYLINDRICAL
C            BETA  RAY SOURCE. 3/28/78.
C           USE AVG OF RATES FROM OPEN AND OBSCURED SECTIONS.
            FRAC=.2116
            WRITE(1,108)
10          READ(1,100)EL,V,RMIN,DR,RMAX
            RO=1.5095E-08
            EMR=.64608
            EO=.0135
            READ(1,104)TF
            TF=1.745E-02*TF
            DUM=EO*((1.+(TF+RMIN*1.3E-03)/RO)**EMR-1.)
            WRITE(1,105)DUM
            READ(1,101)NX,NE,EMIN
            DX=EL/FLOAT(NX)
            EM1=1.5478
            EMU=-.35392
            ES=300.
            EM=670.
            EMS=370.
            VL=1.303E+11/EL
            DE=(EM-EMIN)/FLOAT(NE)
            WRITE(1,107)DE
            R=RMIN-DR
20          R=R+DR
            IF(R-RMAX)25,25,10
25          T=TF+R*1.3E-03
            QEI=0
            WRITE(1,106)
            DO 80 I=1,NX
            X=DX*(FLOAT(I)-.5)
            SQ=SQRT(1.+((X-V)/R)**2)
            DUM=SQ*T/RO
            ER=EO*((1.+DUM)**EMR-1.)
            QEJ=0
            DO 60 J=1,NE
            EJ=EMIN+DE*(FLOAT(J)-.5)
            IF(EJ-ER)60,60,30
30          FJ=((1.+EJ/EO)**EM1-DUM)**EMU
            EN=1.
            IF(EJ-ES)40,40,35
35          EN=(EM-EJ)/EMS
40          QEJ=QEJ+FJ*EN
60          CONTINUE
            QEX=QEJ*VL*DE*FRAC/(R*SQ)**2
            WRITE(1,102)X,QEX,ER
80          QEI=QEI+QEX
            QEI=DX*QEI
            WRITE(1,103)R,QEI
            GO TO 20
100         FORMAT('L='F5.1//'V='F5.1//'RMIN='F5.1//'DELR='F5.1//'RMAX='F5.1)
101         FORMAT('NX='I3//'NE='I3//'EMIN='F5.0)
102         FORMAT(F5.1,E12.4,F7.1)
103         FORMAT(' R='F5.1,' CM    Q/SA='E11.4' IONS/(CM**3-SEC-CURIE)'/)
104         FORMAT('CU FOIL THICKNESS,MILS='F4.1)
105         FORMAT('FOIL+MIN AIR PATH RANGE ENERGY,KEV='F6.1)
106         FORMAT(/'    X       QX/SA          ER')
107         FORMAT('DELTA E='F4.1' KEV'//' X=CM,'
     1' QX/SA=IONS/(CM**3-SEC-CURIE-CM), ER=KEV'/)
108         FORMAT(////'ALL LENGTHS ARE IN CM, ENERGIES IN KEV'/) ·
            END
```

Table 3. 1 FORTRAN Program CYLION for Calculation of Ionization Rate due to Cylindrical Beta Source.

R CYLION

ALL LENGTHS ARE IN CM, ENERGIES IN KEV

L=30.
V=15.
RMIN=10.
DELR=10.
RMAX=20.
CU FOIL THICKNESS,MILS=2.0
FOIL+MIN AIR PATH RANGE ENERGY,KEV= 214.2
NX=30
NE=230
EMIN=210.
DELTA E= 2.0 KEV

X=CM, QX/SA=IONS/(CM**3-SEC-CURIE-CM), ER=KEV

X	QX/SA	ER
0.5	0.3301E+07	308.8
1.5	0.3566E+07	299.5
2.5	0.4211E+07	290.3
3.5	0.4680E+07	281.2
4.5	0.5541E+07	272.3
5.5	0.6203E+07	263.7
6.5	0.7017E+07	255.3
7.5	0.7979E+07	247.4
8.5	0.9136E+07	240.0
9.5	0.1003E+08	233.3
10.5	0.1110E+08	227.3
11.5	0.1242E+08	222.3
12.5	0.1333E+08	218.4
13.5	0.1368E+08	215.7
14.5	0.1428E+08	214.4
15.5	0.1428E+08	214.4
16.5	0.1368E+08	215.7
17.5	0.1333E+08	218.4
18.5	0.1242E+08	222.3
19.5	0.1110E+08	227.3
20.5	0.1003E+08	233.3
21.5	0.9136E+07	240.0
22.5	0.7979E+07	247.4
23.5	0.7017E+07	255.3
24.5	0.6203E+07	263.7
25.5	0.5541E+07	272.3
26.5	0.4680E+07	281.2
27.5	0.4211E+07	290.3
28.5	0.3566E+07	299.5
29.5	0.3301E+07	308.8

R= 10.0 CM   Q/SA= 0.2530E+09 IONS/(CM**3-SEC-CURIE)

Table 3.2 Input to Program CYLION and Output for R = 10 cm.

X	QX/SA	ER
0.5	0.1844E+07	286.7
1.5	0.1927E+07	282.4
2.5	0.2040E+07	278.3
3.5	0.2172E+07	274.3
4.5	0.2334E+07	270.6
5.5	0.2346E+07	267.1
6.5	0.2515E+07	263.9
7.5	0.3147E+07	261.0
8.5	0.2788E+07	258.4
9.5	0.2859E+07	256.1
10.5	0.2954E+07	254.2
11.5	0.3087E+07	252.6
12.5	0.3024E+07	251.4
13.5	0.3187E+07	250.6
14.5	0.3149E+07	250.2
15.5	0.3149E+07	250.2
16.5	0.3187E+07	250.6
17.5	0.3024E+07	251.4
18.5	0.3087E+07	252.6
19.5	0.2954E+07	254.2
20.5	0.2859E+07	256.1
21.5	0.2788E+07	258.4
22.5	0.3147E+07	261.0
23.5	0.2515E+07	263.9
24.5	0.2346E+07	267.1
25.5	0.2334E+07	270.6
26.5	0.2172E+07	274.3
27.5	0.2040E+07	278.3
28.5	0.1927E+07	282.4
29.5	0.1844E+07	286.7

R= 20.0 CM   Q/SA= 0.7874E+08 IONS/(CM**3-SEC-CURIE)

Table 3.3 Output of Program CYLION for R = 20 cm.

23

4. CHARGE GENERATION AND SEPARATION

The generation and separation of charge takes place in one cylindrical section, as shown in Figs. 2.1 and 2.2. The idealized geometry of one segment of this cylinder is shown in Fig. 4.1. The ^{85}Kr produces ionization in the central portion of the segment, with a potential V_o (volts) across the section edge plates. For simplification in the theoretical analysis of the charge separation, the reduced variable y (range 0 to 1) is introduced, and plane parallel geometry is assumed with the separation $d = R\theta$ being a (variable) parameter.
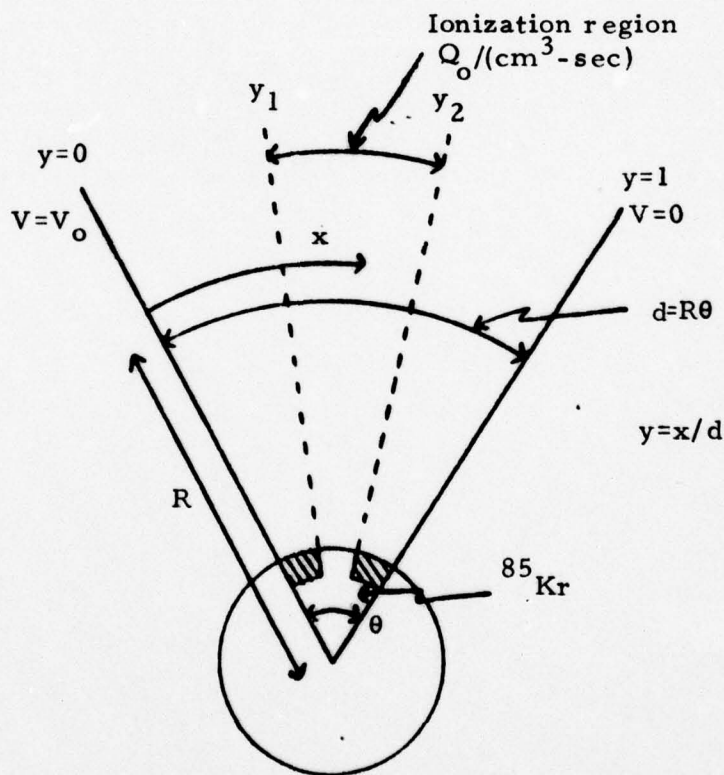

Fig. 4.1. Geometry of Charge Generation and Separation Section.

24

The charge density and electric field equations can be written as

$$-\left(\frac{Dn_o}{Q_o d^2}\right)\frac{d^2 N_+}{dy^2} + \left(\frac{\mu E n_o}{Q_o d}\right)\frac{dN_+}{dy} = \frac{Q}{Q_o} - \left(\frac{\alpha n_o^2}{Q_o}\right)N_+ N_-$$

$$-\left(\frac{4\pi e\mu n_o^2}{Q_o}\right) N_+(N_+ - N_-) \tag{4.1}$$

$$-\left(\frac{Dn_o}{Q_o d^2}\right)\frac{d^2 N_-}{dy^2} - \left(\frac{\mu E n_o}{Q_o d}\right)\frac{dN_-}{dy} = \frac{Q}{Q_o} - \left(\frac{\alpha n_o^2}{Q_o}\right)N_+ N_-$$

$$+\left(\frac{4\pi e\mu n_o^2}{Q_o}\right) N_-(N_+ - N_-) \tag{4.2}$$

and

$$\frac{dE}{dx} = (4\pi e n_o)(N_+ - N_-) \tag{4.3}$$

where D is the diffusion coefficient, $Q_o \simeq 10^{11}/(cm^3 \text{-} sec)$ is the estimated ion pair production rate at (typically) R = 10 cm (Sec. 3), $n_o = \sqrt{Q_o/\alpha} \approx 2.4 \times 10^8/cm^3$ is the zero field equilibrium ion density for a recombination coefficient $\alpha \approx 1.7 \times 10^{-6}$ cm^3/sec for air, $\mu \simeq 1$ cm^2/(V-sec) is the ion mobility in air, and $N_\pm = n_\pm/n_o$ are the normalized positive/negative ion densities, E is the electric field, and d and y are as defined in Fig. 4.1. We define

$$\left.\begin{aligned} \phi_o &= \frac{\mu n_o V_o}{Q_o d^2} = \frac{\mu V_o}{d^2 \sqrt{Q_o d}} \\ &\simeq V_o \text{(volts)}/41231, \text{ for } d = 10 \text{ cm,} \end{aligned}\right\} \tag{4.4}$$

neglect the diffusion term (D/d $\ll \mu$E for reasonable E), and obtain

25

$$\phi_o \frac{E}{E_o} \frac{dN_+}{dy} \simeq \frac{Q}{Q_o} - N_+ N_- - PN_+^2 + PN_+ N_- \tag{4.5}$$

$$- \phi_o \frac{E}{E_o} \frac{dN_-}{dy} \simeq \frac{Q}{Q_o} - N_+ N_- - PN_-^2 + PN_+ N_- \tag{4.6}$$

where $P = 4\pi \dot{\mu} e n_o^2 / Q_o = 4\pi \mu e/\alpha \simeq 1.06$ and $E_o = V_o/d$.

The $N_+ N_-$ terms in (4.5) and (4.6) drop out if $P = 1$, and since P is very nearly 1.0, we set $P = 1.0$ and obtain a simplified set of equations (an approach consistent with the present feasibility determination):

$$\phi_o \frac{E}{E_o} \frac{dN_+}{dy} \simeq \frac{Q}{Q_o} - N_+^2 \tag{4.7}$$

$$- \phi_o \frac{E}{E_o} \frac{dN_-}{dy} \simeq \frac{Q}{Q_o} - N_-^2 \tag{4.8}$$

and

$$\frac{d^2\phi}{dy^2} = N_- - N_+ \tag{4.9}$$

where $\phi = \mu n_o V/(Q_o d^2)$, with V the potential at position y.

Consider the situation of Fig. 4.1, where $Q=0$ for $0 \le y < y_1$, and $y_2 < y \le 1$, and $Q=Q_o$ for $y_1 \le y \le y_2$. For this case the solution to (4.7), (4.8) and (4.9) can be written as:

$0 \le y \le y_1$: $\quad N_+ = 0$

$$N_- = \left[\frac{1}{N_o} + \int_0^y \frac{dy}{-d\phi/dy} \right]^{-1} \tag{4.10}$$

$y_1 \le y \le y_2$: $\quad N_+ = \tanh\left[\int_{y_1}^y \frac{dy}{-d\phi/dy} \right]$

$$\tag{4.11}$$

$$N_- = \tanh\left[\int_y^{y_2} \frac{dy}{-d\phi/dy} \right]$$

26

$y_2 \leq y \leq 1$:

$$N_+ = \left[\frac{1}{N_o} + \int_{y_2}^{y} \frac{dy}{-d\phi/dy} \right]^{-1}$$

$$N_- = 0$$

(4.12)

where

$$N_o = \tanh \left[\int_{y_1}^{y_2} \frac{dy}{-d\phi/dy} \right]$$

(4.13)

The set of equations (4.10) to (4.13) can be used to solve for N_+, N_-, and ϕ, all as functions of y, by splitting $0 \leq y \leq 1$ into several segments and numerically solving for the values at each breakpoint. This has been done for 16 breakpoints (including y=0 and 1), and the results for N_+ and N_- are plotted in Fig. 4.2 for three values of ϕ_o. Only one N_- profile has been plotted, since all N_- profiles are the N_+ profiles reflected about y=0.5. Note that the results imply that some optimum value of ϕ_o exists which maximizes $N_+(y=1)$.

The net charge separation $(N_+ - N_-)$ is plotted in Fig. 4.3. As a result of the method of normalizing to n_o, the results do not depend explicitly on Q, the ion-electron production rate. Q must be determined analytically and experimentally to allow more accurate calculations for N_+, N_-. Figure 4.3 shows that while small ϕ_o maximizes the charge separation at $y = y_1, y_2$, the maximum integrated charge separation is for some intermediate value of ϕ_o. The best value of ϕ_o is that which maximizes

$$N_{sep} = \int_{0.5}^{1} (N_+ - N_-)dy$$

(4.14)

and this can be readily done by numerical calculations. Because of the normalization of N_+ and N_- to n_o, there is a single optimum for ϕ_o, and the corresponding V_o can be readily determined from Eq. (4.4) for any set of parameters d, etc. Since d and $n_o = \sqrt{Q_o/\alpha}$ vary somewhat with R (see Fig. 4.1), the optimum V_o varies slightly with R, and a suitable average value will have to be selected. From Fig. 4.3 it can be seen that net charge concentrations

27
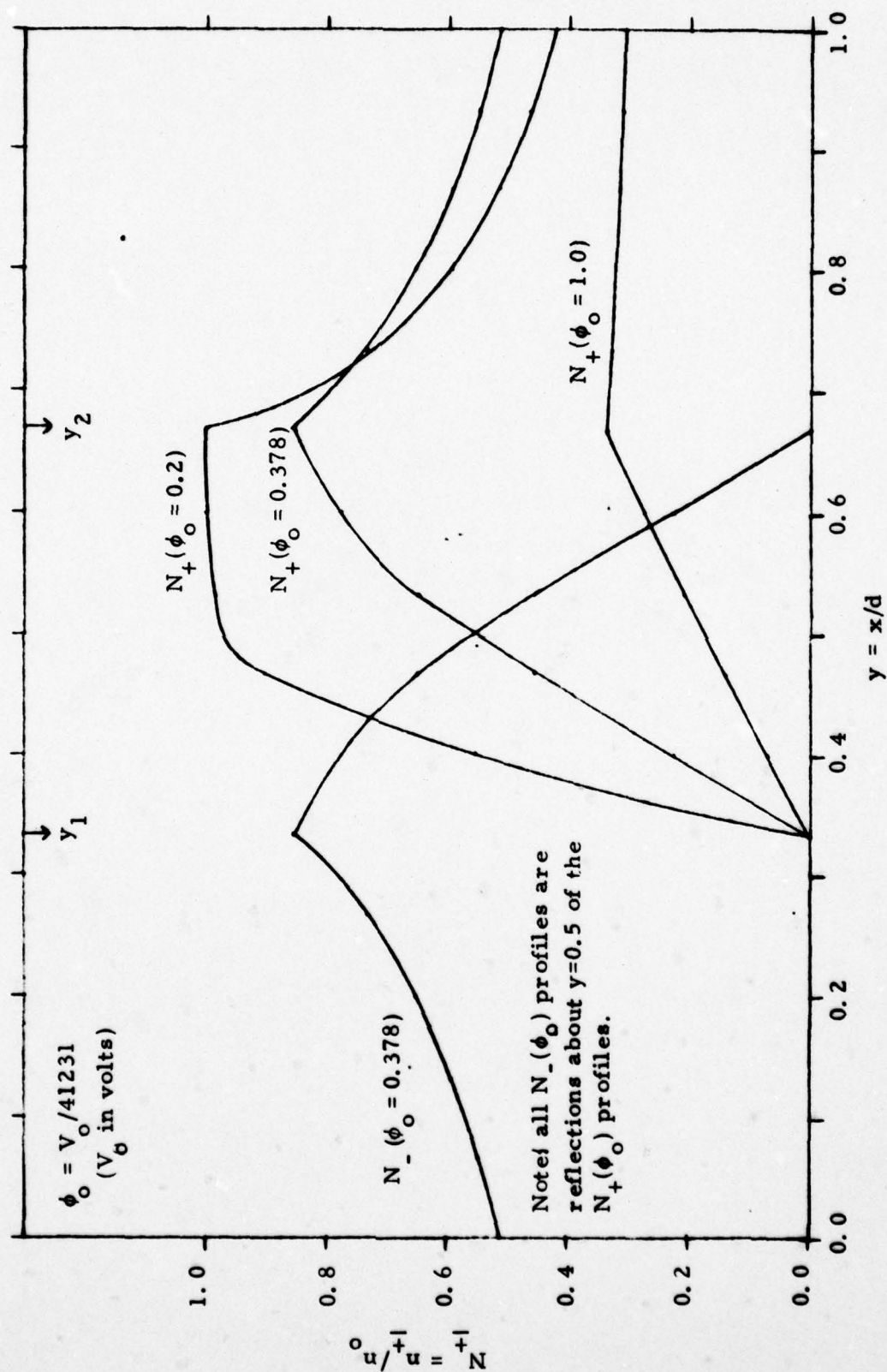
Fig. 4.2. Charge distribution for three voltages.

28
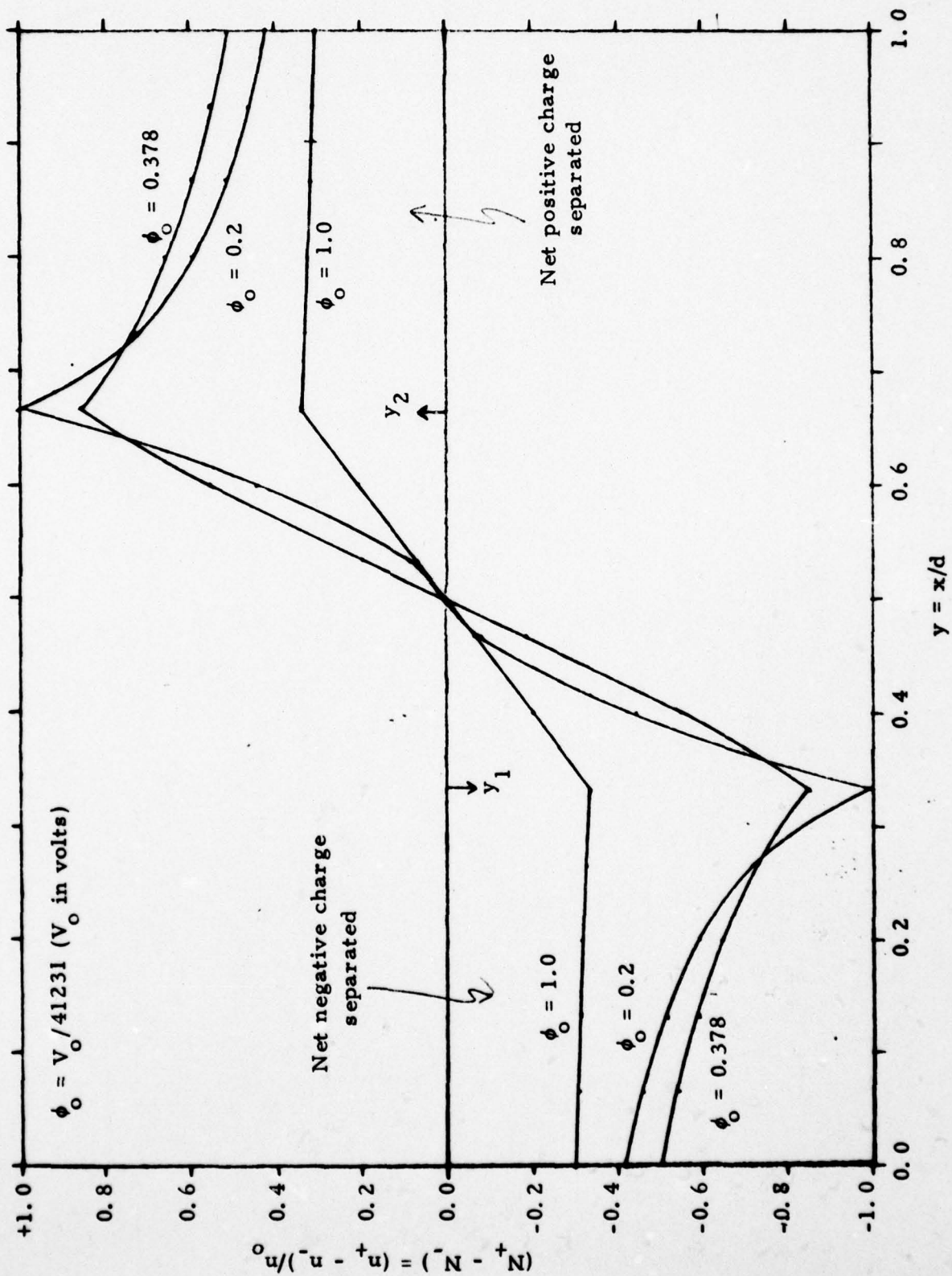
Fig. 4.3. Net charge density distribution for three voltages.

29

of $> 0.5\ n_o$ can be achieved in the separation regions, so that separated charge densities of more than half the equilibrium electron-ion density n_o can be achieved. That these densities will be sufficient to induce an amount of charge on particulates that will cause significant agglomeration in that section of the device is investigated in Section 5.

4.1

The geometry of Fig. 4.1 is idealized, since in practice the ionization region will not have sharp boundaries. Indeed, the results of Section 3 show that beta particle scattering produces very significant effects. However, the theoretical analysis shows that significant charge separation can be achieved and gives numerical values for the approximate optimum potential V_o. This helps significantly in guiding any experimental work done in the next stage of work.

5. PARTICLE CHARGING AND AGGLOMERATION

In this section we consider how the particles are charged in the charger (Sec. 5.1) and how they are then agglomerated in the agglomerator (Sec. 5.2). We assume (a) that there are essentially two populations: "small" particles below about one micrometer in radius (subscripts 1), and "large" particles above about one micrometer in radius (subscripts 2); and (b) that the small particles agglómerate onto the large particles.

5.1 Charging Section

In the charging section we assume that the particles find themselves in a charging environment where there are unipolar ions of density n_+, and an electric field of intensity E_{ch}. We assume the particles are exposed to this environment for an interval of one second. (The results are insensitive to the exact value of this time interval.) For small particles, the charging is generally dominated by the "diffusion" mechanism, while for large particles the charging is generally dominated by the "field" (conduction) charging mechanism (Ref. 5.1,5.2). For the present purposes, we assume here that the small and large particles are charged only by diffusion and conduction, respectively.

5.1.1 Diffusion Charging

For diffusion charging, which is appropriate for small particles, the number of elementary charges acquired in time t is given [Ref. 5.1, Eq. (3.61); Ref. 5.2, Eq. (5.27)] by:

$$n_1 = \frac{RkT}{e^2} \ln\left(1 + \frac{t}{\tau_D}\right) \tag{5.1}$$

where

$$\tau_D = \frac{kT}{\pi e^2 U_i n_+ R} \tag{5.2}$$

where R is the radius of the particle, n_+ is the undisturbed ion density, e is the magnitude of the electron charge, U_i is the rms thermal velocity of the ions, k is Boltzmann's constant, and T is the absolute temperature. At room tem-

31

perature, we take $kT = 4 \times 10^{-14}$ erg and $U_i = 5 \times 10^4$ cm/sec for nitrogen molecules, and we may write:

$$\frac{e^2}{RkT} = \frac{5.76 \times 10^{-6}}{R} \tag{5.3}$$

$$\tau_D = \frac{1}{0.905 n_+ R} \text{ sec} \tag{5.4}$$

$$n_1 = 1.736 \times 10^5 R \ln(1 + 0.905 n_+ R t) \tag{5.5}$$

Assuming (a) the optimum value of E_{ch} for separating the positive and negative ions (given by $\phi_o \cong 0.378$ in Section 4), (b) a distance of $d = 10$ cm = arc length between the plates, and (c) a local source ionization rate of $Q_o = 10^{11}$ ion pairs per cm^3 per sec, we obtain a value $n_+ \cong 1.5 \times 10^8 cm^{-3}$ for ion density, at a voltage of about 15600 volts across the plates and a field intensity of $E_{ch} = 5.2$ statvolts/cm. (The value of n_+ is the average value of the ion density profile, that is, about 60% of the nominal ion density $n_o = \sqrt{Q_o/\alpha}$, where Q_o is the ionization rate $= 10^{11} cm^{-3} sec^{-1}$, and α is the recombination coefficient $= 1.7 \times 10^{-6} cm^3 sec^{-1}$.)

For particles of radius $R = 0.1$ micrometer, and $n_+ = 1.5 \times 10^8 cm^{-3}$, Eq. (5.1) becomes

$$n_1 = 1.736 \ln(1 + 1358t) \tag{5.6}$$

$$= 12.52 \text{ charges in one second.}$$

Note that this charging is insensitive to the time t and to the ion density n_+ because of the logarithm. It is explicitly independent of the charging field E_{ch}, but n_+ depends on this as seen in the previous section.

5.1.2 Conduction (or Field) Charging

For conduction (or "field") charging, which is appropriate for large particles, the number of elementary charges of magnitude e acquired in time t is given [Ref. 5.1, Eq. (3.58); Ref. 5.2, Eq. (5.15)] by:

$$n_2 = n_{sat}\left(\frac{t}{t + \tau_c}\right) \tag{5.7}$$

32

where

$$\tau_c = \frac{1}{\pi e \mu n_+} = 2.210 \times 10^6 / n_+ \text{ sec} \qquad (5.8)$$

and

$$n_{sat} = 3R^2 E_{ch}/e = 6.25 \times 10^9 E_{ch} R^2 \qquad (5.9)$$

where n_{sat} denotes the "saturation" charge, a finite value attained after an infinite time, with the time-scale given by τ_c. Equation (5.8) for τ_c is obtained assuming $\mu = 1 \text{ cm}^2/\text{volt-sec} = 300 \text{ cm}^2/\text{sv-sec}$. For practical purposes, $n = n_{sat}$ may be considered the value of n_2 after a few time periods τ_c. Note that n_{sat} does not depend on n_+, while τ_c essentially depends only on n_+ and is independent of R and E_{ch}. For ion density $n_+ = 1.5 \times 10^8 / \text{cm}^3$, τ_c is only 0.015 sec so that on a time scale of the order of seconds all large particles have $n_2 \cong n_{sat}$. (The factor 3 is Eq. (5.9) is for conducting particles; for nonconducting particles this factor is between unity and 3, depending on the dielectric constant.) For $R = 0.1 \mu m$ and $E_{ch} = 5.2 \text{ sv/cm}$, $n_2 = 3.25$ by conduction compared with $n_1 = 12.52$ obtained with one second of diffusion charging. For $R = 1.0 \mu m$ and the same E_{ch}, $n_2 = 325$ by conduction charging compared with $n_1 = 165$ by diffusion charging. At $R = 0.468 \mu m$ we have $n_1 = n_2 = 71.1$. Hence, the transition between diffusion and conduction as the dominant charging mechanism occurs in the range $R = 0.1 \mu m$ to $R = 1.0 \mu m$. Thus, both mechanisms are important in contributing to the charge in this critical range. However, since we are interested in all values of R below $1.0 \mu m$ (all submicron particles), we will be on conservative ground if we assume that diffusion alone is responsible for the charging of all submicron particles.

The charging theories used for the estimates of this report are the standard simplified theories. There exist more complicated theories which combine the diffusion and conduction mechanisms (Ref. 5.3), but their use would not change the numbers significantly and seems unjustified for our present purposes.

The large particles are assumed to act as collectors and to be described by a log-normal distribution. Among the quantities needed in the theory of the agglomeration process to be considered next are the average values of n and of

Bn, where B is the particle mobility assumed to be given by the Stokes viscous drag law:

$$B = \frac{C(R)}{6\pi\eta R} \left(\frac{sec}{g}\right) \qquad (5.10)$$

where η is the dynamic viscosity of air (which we take to be 1.8×10^{-4} poise or g/cm/sec at room temperature), and $C(R)$ is the Cunningham "slip" factor which accounts for the fact that the particle is not large compared with the collisional mean free paths of the air molecules. The latter factor has been given as (Refs. 5.4, 5.5):

$$\left.\begin{array}{l} C(R) = 1 + [1.257 + 0.4 \exp (-1.1R')] / R' \\[2mm] \text{with } R' = R/6.62 \times 10^{-6} = R(\mu m)/0.0662 \end{array}\right\} \qquad (5.11)$$

Table 5.1 shows how $C(R)$ varies with R. Above $R = 1.0 \mu m$, $C(R)$ is essentially unity. Below $R = 0.1 \mu m$, $C(R)$ rises approximately as R^{-1}. Table 5.1 also shows the product of B and n ($B_1 n_1$ for "small" particles), where n is obtained from the diffusion-charging formula [Eq. (5.5)] with $n_+ = 1.5 \times 10^8/cm^3$ and $t = 1$ sec. It is important to note that the product Bn is almost constant in the range $R = 0.1 \mu m$ to $R = 1.0 \mu m$. Thus, since the agglomeration theory to be described next involves n_1 through the product $B_1 n_1$ for small particles, the results will be insensitive to R_1 in the range $0.1 \mu m$ to $1.0 \mu m$.

5.2 Agglomerator Section

The air flowing into the agglomerator section is loaded inhomogeneously with charged particles, such that there are essentially only positive charges on one side, and negative charges on the other side. There is a superimposed electric field of intensity E in this section whose purpose is to pull the oppositely-charged clouds of particles toward each other and to mix them, so that oppositely-charged partners can come together and agglomerate. The task of this section is to determine the time-scales under which the two processes occur: transit across the gap, and agglomeration.

34

TABLE 5.1

Variations of $C(R)$ and $B_1 n_1$ with R*

(Assumes $n_+ = 1.5 \times 10^8 / cm^3$, t = 1 sec diffusion charging)

$R (\mu m)$	$C(R)$	$B_1 n_1$	B_1	n_1	n_{sat}
0.0	∞	7.620×10^{10}	∞	0	0
0.001	110.26	1.512×10^{10}	3.250×10^{11}	0.0465	0.000325
0.01	14.93	3.757×10^{9}	4.400×10^{9}	0.854	0.0325
0.1	1.882	6.949×10^{8}	5.547×10^{7}	12.52	3.25
0.2	1.421	5.749×10^{8}	2.094×10^{7}	27.45	13.0
0.3	1.278	5.436×10^{8}	1.256×10^{7}	43.29	29.25
0.4	1.208	5.316×10^{8}	8.901×10^{6}	59.72	52.0
0.5	1.166	5.266×10^{8}	6.873×10^{6}	76.58	81.25
0.6	1.139	5.247×10^{8}	5.595×10^{6}	93.80	117.0
0.65	1.128	5.244×10^{8}	5.115×10^{6}	102.5	137.3
0.7	1.119	5.244×10^{8}	4.711×10^{6}	111.3	159.3
0.8	1.104	5.250×10^{8}	4.067×10^{6}	129.1	208.0
0.9	1.093	5.261×10^{8}	3.579×10^{6}	147.0	263.3
1.0	1.083	5.275×10^{8}	3.192×10^{6}	165.2	325.0
2.0	1.042	5.441×10^{8}	1.536×10^{6}	354.5	1300.

*R = particle radius

$C(R)$ = Cunningham slip factor

B_1 = particle mobility

n_1 = particle charge (number of elementary charges) by diffusion

n_{sat} = saturation charge by conduction at E = 5.2 sv/cm

5.2.1 Agglomeration

We wish to consider two clouds of oppositely-charged particles, moving past each other with constant velocity, and to determine the probability of a contact occurring. In particular, we consider a large particle acting as a collector, with a reference frame fixed on this collector. The other particles stream past it at velocity v_o, so that we can determine the collection efficiency by analyzing the orbits of the streaming particles and counting those which intersect the collector. To do this analytically, we assume that the collected particles are inertia-less, that is, their inertial acceleration is negligible compared with, say, that due to viscous drag (demonstrated by calculations in Ref. 5.5; see also Ref. 5.2, p. 36). An appropriate analysis for this problem approximates the orbit by that resulting from a constant velocity v_o superimposed on the velocity due to a central force. If these velocities are sufficiently large, it can be shown that Brownian diffusion can be neglected (Ref. 5.5). (That is, including Brownian diffusion will lead to the same result in the limit of large charges - see Sec. 5.1.2.)

In Fig. 5.1, we depict the collection of small particles of radius R_1 by a large particle of radius R_2, under an attractive central force of magnitude K_p/r^p between the particles, with p denoting the exponent for a power-law force, and K_p the associated constant; v_o denotes the relative velocity = $(B_1 n_1 + B_2 n_2)eE$. There are 3 types of orbits portrayed, Type A representing uncollected particles, Type B representing collected particles, and Type C representing the critical orbit dividing the two classes of orbits. If we can determine x_o, the initial offset distance of the critical orbit, then the collection efficiency is given by $\mathcal{E} = x_o^2/(R_1 + R_2)^2$. To compute x_o we write the equations for the orbits in the form

$$\vec{v} = \vec{v_o} - (K_p/r^p)\hat{r} \tag{5.12}$$

$$\frac{dr}{dt} = v_r = -v_o \cos\theta - K_p/r^p \tag{5.13}$$

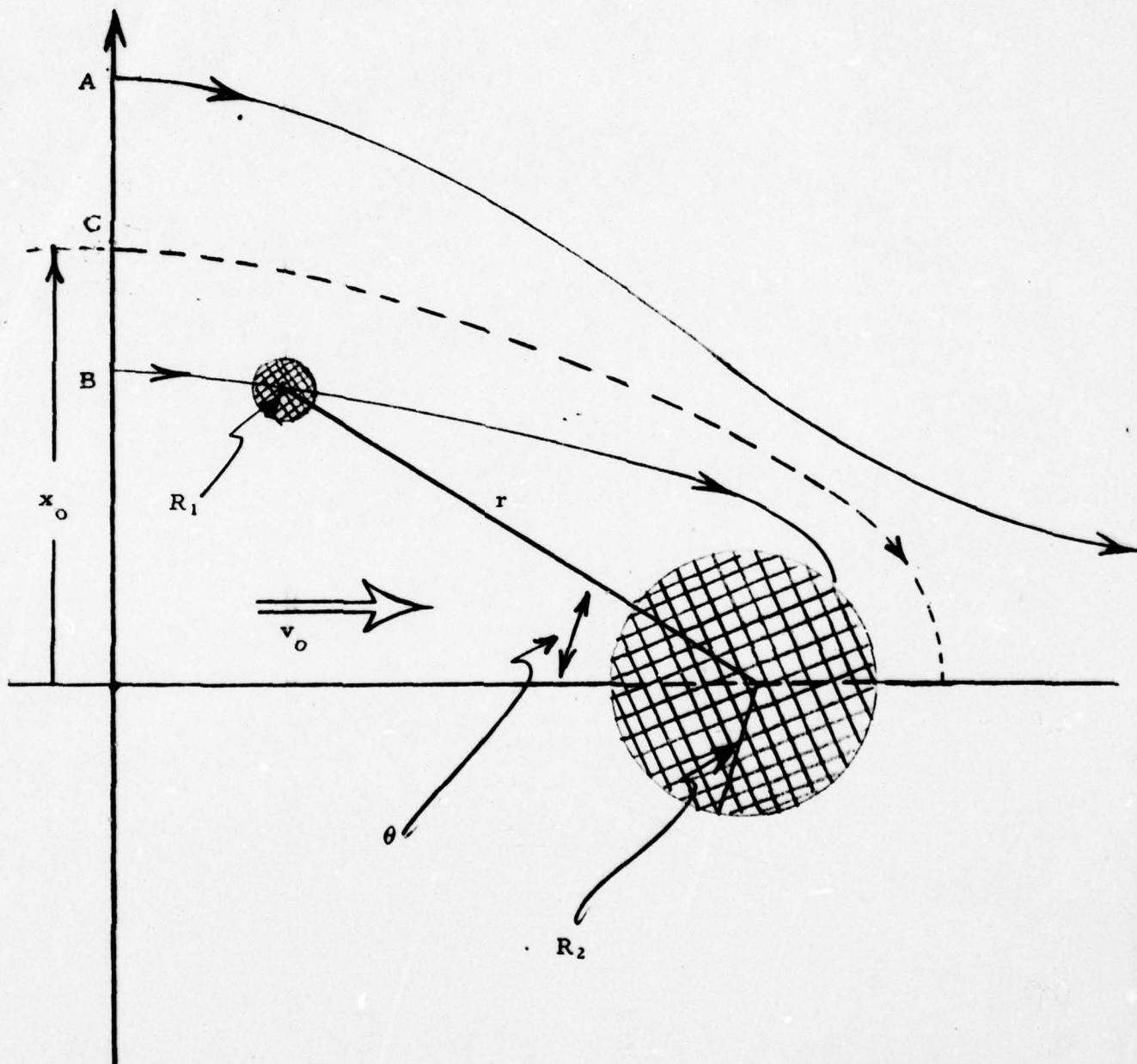$$r\frac{d\theta}{dt} = v_\theta = v_o \sin\theta \tag{5.14}$$

36

Fig. 5.1 Collection of Small Particles by a Large Particle

From these equations the shape of the orbit is given by

$$\frac{1}{r}\frac{dr}{d\theta} = -\cot\theta - \frac{K_p}{v_o r^p \sin\theta} \tag{5.15}$$

from which we obtain the solution

$$x^p = x_o^{\ p} - \frac{pK_p}{v_o}\int_0^\theta \sin^{p-1}\theta d\theta \tag{5.16}$$

where $x \equiv r\sin\theta$

The critical orbit is that for which x vanishes when $\theta = \pi$, that is, the right-hand side vanishes. Thus, we have the critical value of x_o:

$$x_o = \left[\frac{pK_p}{v_o}\int_0^\pi \sin^{p-1}\theta d\theta\right]^{1/p} \tag{5.17}$$

and the collection efficiency may be written:

$$\mathcal{E}_p = \frac{x_o^{\ 2}}{(R_1+R_2)^2} = \frac{1}{(R_1+R_2)^2}\left[\frac{pK_p}{v_o}\int_0^\pi \sin^{p-1}\theta d\theta\right]^{2/p} \tag{5.18}$$

For a Coulomb force of attraction between the two particles (the case of interest here), p and K_p are given by p=2 and $K_p = B_1 n_1 n_2 e^2$, where n_1 and n_2 are the numbers of elementary charges on the particles. The collection efficiency is

$$\mathcal{E}_2 = \frac{4B_1 n_1 n_2 e^2}{v_o(R_1+R_2)^2} \tag{5.19}$$

If η_1 and η_2 denote the density of small particles and large particles, respectively, the rate of disappearance of small particles per unit volume, $d\eta_1/dt$, is given by multiplying $\mathcal{E}_2$ by η_2 and by the current of small particles $\pi(R_1+R_2)^2 v_o \eta_1$:

38

$$\frac{d\eta_1}{dt} = -4\pi \eta_1 \eta_2 B_1 n_1 n_2 e^2 = -\frac{\eta_1}{\tau_A} \tag{5.20}$$

Thus, τ_A represents the agglomeration time

$$\tau_A = (4\pi \eta_2 B_1 n_1 n_2 e^2)^{-1} \tag{5.21}$$

which is seen to be independent of E (through v_0). Assuming η_2 constant, this implies an exponential decay of the small-particle population, with time-constant τ_A, due to agglomeration onto the large particles.

If the small particles have no charge, they are still attracted to the charged large particles by the polarization force which is inversely proportional to the fifth power of the inter-particle distance. (Ref. 5.5). In this case we set p=5 in Eq. (5.18), and $K_5 = 2R_1^3 B_1 n_2^2 e^2$. Evaluating the integral and deriving an equation of form similar to Eq. (5.20), we find that the agglomeration time for the neutral-small-charged-large-particle case is given by

$$\tau_A' = \eta_2^{-1} \left[\frac{15}{4} \pi^{7/2} v_0^{3/2} B_1 R_1^3 n_2^2 e^2 \right]^{-2/5} \tag{5.22}$$

which is (of course) independent of n_1, and which depends on E through $v_0 = (B_1 n_1 + B_2 n_2)eE$. This 2/5-power-law result corresponds to the asymptotic limit of results obtained previously by Parker (Ref. 5.5) using boundary-layer analysis to take into account fluid-flow effects in the collection of uncharged aerosols by charged droplets.

5.2.2 Thermal Agglomeration

The formula for agglomeration time τ_A, Eq. (5.21), was derived by assuming inertia-less particles and neglecting diffusion. Zebel (Ref. 5.6) treats the agglomeration of charged aerosol particles undergoing Brownian diffusion. For two types of particles, of radius, mobility, and charge R_1, B_1, and $n_1 e$, and R_2, B_2, and $n_2 e$, the ratio of thermal agglomeration rates (or "coagulation constants") for charged and uncharged particles is a factor

39

$$f = \frac{y}{(1 + G_o y)\exp(y) - 1} \tag{5.23}$$

where

$$y = \frac{n_1 n_2 e^2}{(R_1 + R_2)kT} \tag{5.24}$$

and G_o is a gas-kinetic correction factor which vanishes for large particles and which introduces finite mean-free-path effects for small particles. The variable y describes the electrical force between the charged particles; it vanishes for neutral particles and is large for large forces, positive for repulsion and negative for attraction. For strongly-charged aerosols ($|y|$ large), the increase due to attraction exceeds the decrease due to repulsion and results in a net significant increase in agglomeration. For large negative y, f becomes equal to $|y|$. Thus, since the neutral agglomeration rate per unit volume is

$$K_o = 4\pi(B_1 + B_2)(R_1 + R_2)kT \mathcal{N}_1 \mathcal{N}_2 \tag{5.25}$$

the net agglomeration rate is

$$K_o f = 4\pi(B_1 + B_2)n_1 n_2 e^2 \mathcal{N}_1 \mathcal{N}_2 \tag{5.26}$$

which corresponds to the right-hand side of Eq. (5.20) if we neglect B_2 compared with B_1 (which should be justified if B_2 and B_1 are associated with large and small particles, respectively).

5.2.3 Electrostatic Dispersion or Mutual Repulsion

Another effect which needs to be considered is that due to the charges within the two oppositely-charged clouds of unipolar particles before they are brought together in the agglomerator. Each cloud will tend to expand and disperse to the walls as the particles recede from each other under their mutual repulsions. In particular, we desire to know the time-scale under which the large particles, which are to act as collectors, will disperse. The decrease in concentration of

a spatially-homogeneous cloud of large particles (but with distributed sizes) is given by

$$\frac{\partial \eta_2}{\partial t} = -\text{div}(\eta_2 \vec{v}) = -\eta_2 B_2 n_2 \, e \, \text{div} \vec{E}$$

$$= -\eta_2 B_2 n_2 \, e \cdot 4\pi e \sum_j \eta_j n_j$$

$$= -\eta_2 B_2 n_2 \cdot 4\pi e^2 \eta_o \bar{n}$$

$$= -\eta_2 / \tau_R \tag{5.27}$$

where η_o is the total number of particles per unit volume and $\bar{n}$ is the average number of charges on a particle. Thus, the average repulsion time of a cloud of distributed sizes and charges may be taken to be:

$$\tau_R = (4\pi \eta_o \overline{B_2 n_2} \cdot \bar{n} e^2)^{-1} \tag{5.28}$$

where $\overline{B_2 n_2}$ is the average value of $B_2 n_2$ in the cloud.

Thus, the particle clouds must be brought together within a time less than τ_R in order to get them mixed so they can agglomerate. Once mixed, they will require a time of order τ_A to agglomerate significantly. Formulas for τ_A and τ_R useful for system design purposes will be presented in the next section, where particle size distributions are taken into account.

5.3 Particle Size Distributions and Design Criteria

Although theoretical analyses are simpler when the particle size distributions are monodisperse, in actual cases it is necessary to deal with polydisperse aerosol systems. Such systems are usually described by log-normal distributions. The properties of log-normal distributions are well known (e.g., Ref. 5.1, Chap. 5). In this section we will replace functions of particle diameter D by mean values of these functions based on the log-normal distribution.

Typically, particle distributions are defined by the mass median diameter (here denoted by $D_{m/2}$) and the geometric standard deviation (here denoted by σ_g). All other special quantities of interest may be derived from these. Among the special quantities are the following:

D_g = count median or geometric mean diameter = $D_{m/2} \exp(-3 \ln^2 \sigma_g)$

$\overline{D}$ = count mean diameter (or simply "mean diameter") = $D_g \exp(0.5 \ln^2 \sigma_g)$

$\overline{D^2}$ = count mean square diameter (average area) = $D_g^2 \exp(2 \ln^2 \sigma_g)$

$\overline{D^3}$ = count mean cube diameter (average volume) = $D_g^3 \exp(4.5 \ln^2 \sigma_g)$

F_1 = relative number (or fraction) of particles with diameter D less than D_1 (fraction of "small" particles)

= $0.5 \, \text{erfc} \, [(\ln D_g - \ln D_1)/\sqrt{2} \ln \sigma_g]$

F_2 = relative number (or fraction of particles with diameter D greater than D_1 (fraction of "large" particles)

= $0.5 \, \text{erfc} \, [(\ln D_1 - \ln D_g)/\sqrt{2} \ln \sigma_g]$

= $1 - F_1$

5.3.1 Agglomeration Time

The agglomeration time τ_A is given by Eqs. (5.20) and (5.21). We will replace η_2 by $F_2 \eta_0$, where η_0 is the total number of particles per cm³, and η_0 by

$$\eta_0 = \frac{\mathcal{M}}{\frac{4\pi}{3} \rho \overline{R^3}} = \frac{6}{\pi} \frac{\mathcal{M}}{\rho \overline{D^3}} \tag{5.29}$$

where $\mathcal{M}$ denotes the mass loading in grams of aerosol per cm³ of air, ρ is the solid density of the aerosol (here taken to be 2 gm/cm³), and $\overline{D^3}$ is the mean cube of the particle diameter. We also replace n_2 by the mean value of n_{sat}, which is (Eq. (5.9)):

$$\overline{n}_{sat} = 3\overline{R^2} E_{ch}/e = 3\overline{D^2} E_{ch}/4e \tag{5.30}$$

42

where $\overline{D^2}$ is the mean square of the particle diameter. Then τ_A may be written:

$$\tau_A \mathcal{M} = \left(\frac{\rho}{18 e\, E_{ch}\, B_1 n_1} \right) \left(\frac{\overline{D^3}}{F_2\, \overline{D^2}} \right) \tag{5.31}$$

where the second parentheses depends only on the distribution. Note that $B_1 n_1$ depends only on D_1 ($= 2R_1$), and that τ_A is inversely proportional to the mass-loading parameter $\mathcal{M}$. We take $\rho = 2$ gm/cm^3 and $E_{ch} = 5.2$ sv/cm, and assume $R = 0.1 \mu$m so that $B_1 n_1 = 6.949 \times 10^8$ (Table 5.1). Then Eq. (5.31) may be written:

$$\tau_A \mathcal{M} = 6.406 \times 10^{-6} \left(\frac{\overline{D^3}}{F_2\, \overline{D^2}} \right) \tag{5.32}$$

$$(R = 0.1 \mu m) \qquad\qquad \text{in } \mu m$$

It is important to note that, while τ_A is evaluated here only for $R = 0.1 \mu$m, the dependence on R is through $B_1 n_1$, which, as Table 5.1 shows, is nearly constant in the R-range 0.1μm to 1.0μm.

5.3.2 Repulsion Time

The mutual repulsion time τ_R is given by Eqs. (5.27) and (5.28). We replace η_o by Eq. (5.29), and $\overline{n}$ by $\overline{n}_{sat}$ as in Eq. (5.30). The average value of $B_2 n_2$ is replaced by

$$\overline{B_2 n_2} = \overline{\left(\frac{1}{3\pi\eta D} \cdot \frac{3 E_{ch} D^2}{4e} \right)} = \frac{E_{ch}}{4\pi e \eta} \overline{D} \tag{5.33}$$

Then τ_R may be written:

$$\tau_R \mathcal{M} = \left(\frac{2\pi}{9} \frac{\rho\eta}{E_{ch}^2} \right) \left(\frac{\overline{D^3}}{\overline{D^2} \cdot \overline{D}} \right) = 9.295 \times 10^{-6} \left(\frac{\overline{D^3}}{\overline{D^2} \cdot \overline{D}} \right) \tag{5.34}$$

where we have assumed $\rho = 2$, $\eta = 1.8 \times 10^{-4}$, and $E_{ch} = 5.2$, and where the final parentheses depends only on the distribution. As in the case of τ_A, τ_R is

43

inversely proportional to $\mathcal{M}$. The dependence on inverse E_{ch}^2 results from the assumption that for the purposes of estimating repulsion times all particles charge up as large particles, i.e., by conduction alone. This should yield a good estimate of τ_R since most of the charge resides on the large particles, and the error in assigning the wrong value of charge to the small particles should be small.

Note that, after the mixing has been achieved, oppositely-charged large particles will tend to agglomerate with one another. This large-particle agglomeration time is roughly given by τ_R.

5.3.3 Voltage to Bring Oppositely Charged Clouds Together

The voltage required to force the oppositely-charged clouds together across a gap of length d may be written as:

$$V(\text{volts}) = \frac{300\ d^2}{(B_1 n_1 + \overline{B_2 n_2})et}$$

$$= \frac{300\ d^2}{[B_1 n_1 + \overline{D}E_{ch}/(4\pi e\eta)]et} \tag{5.35}$$

where we have used Eq. (5.33) for $\overline{B_2 n_2}$, and the factor 300 is required to convert statvolts to volts. The time t should be τ_A or τ_R, whichever is shorter. We assume that d=10 cm, E_{ch} = 5.2 sv/cm, and $\eta = 1.8 \times 10^{-4}$ poise. Then Eq. (5.35) may be written:

$$V(\text{volts}) = \frac{130500}{[2.088 \times 10^{-9} B_1 n_1 + \overline{D}(\mu m)]t(\text{sec})} \tag{5.36}$$

Specializing to R=0.1μm particles, so that (Table 5.1) $B_1 n_1 = 6.949 \times 10^8$, we obtain

$$V(\text{volts}) = \frac{130500}{[1.451 + \overline{D}(\mu m)]t(\text{sec})} \tag{5.37}$$

44

Note that this formula also can apply to the charging section, in which we assume 15600 volts is applied across 10 cm, and the particles are exposed for one second. Provided $\overline{D}$ is less than 6.91μm, 15600 volts will be insufficient to move the particles across the channel within the charging time of one second. Hence, the small-particle charging can be completed before the particles move to the walls under the applied charging field.

5.3.4 Maximum Loading $\mathcal{M}_{max}$

In the foregoing equations, the mass loading $\mathcal{M}$ is a "free" parameter. It cannot be arbitrarily large, however, since the ions would eventually become depleted and the particles would compete for them. It is of interest to consider the foregoing equations in the light of the maximum loading $\mathcal{M}_{max}$ for a given ion supply (n_+ ions/cm^3). Under conditions where all available ions are deposited on particles, and assuming that most of the charges accumulate on the large particles by conduction, we may estimate $\mathcal{M}_{max}$ by equating $n_+ = \mathcal{N}_2 \overline{n}_{sat} = F_2 \mathcal{N}_o \overline{n}_{sat}$, and using Eq. (5.29) for $\mathcal{N}_o$ and Eq. (5.30) for $\overline{n}_{sat}$. Thus, solving for $\mathcal{M} = \mathcal{M}_{max}$:

$$\mathcal{M}_{max} = \frac{2\pi}{9} \rho e \frac{n_+}{E_{ch}} \left(\frac{\overline{D^3}}{F_2 \overline{D^2}} \right) = 1.933 \times 10^{-6} \underbrace{\left(\frac{\overline{D^3}}{F_2 \overline{D^2}} \right)}_{\text{in } \mu m} \qquad (5.38)$$

where we have used $n_+ = 1.5 \times 10^8/cm^3$, $\rho = 2$ gm/cm^3, and $E_{ch} = 5.2$ sv/cm. Using this value, $\mathcal{M}_{max}$, in the expressions (5.32) and (5.34) for τ_A and τ_R, respectively, we obtain minimal values for τ_A and τ_R, and a maximal value for V from (5.37). The minimal values of τ_A and τ_R are:

$$\left(\tau_A \right)_{min} = (4\pi e^2 n_+ B_1 n_1)^{-1} = 3.31 \text{ sec} \qquad (5.39)$$
$$\text{(for R=0.1}\mu\text{m)}$$

$$\left(\tau_R \right)_{min} = \frac{\eta}{en_+ E_{ch}} \left(\frac{F_2}{\overline{D}} \right) = 4.808 \left(\frac{F_2}{\overline{D}(\mu m)} \right) \text{sec} \qquad (5.40)$$

and $V_{max} < 27170$ volts (for t=3.31 sec and $\overline{D}$=0). It is of interest to note that $\left(\tau_A \right)_{min}$ is independent of the distribution of E_{ch}.

45

5.3.5 Design Criteria

In applying the above formulas to the design of an agglomerator it seems reasonable to assume maximum loading so that $\mathcal{M} = \mathcal{M}_{max}$. This minimizes the agglomeration time τ_A. It also minimizes the self-repulsion time τ_R (which is also approximately the self-agglomeration time for the large particles). The following relations are desirable, namely, that:

(a) τ_A be smaller than τ_R; then agglomeration can occur before self-repulsion (and before self-agglomeration of the large particles).

(b) τ_A be of the order of a second (residence time in the agglomerator section).

(c) V be large enough to bring the particle clouds together and mix them before they disperse by self-repulsion.

(d) E_{ch} (the charging field) be small enough to allow small particles to charge for a second or so before they are pushed to the walls by the charging field (charging section).

In addition, assuming that $F_2/\overline{D}$ is not too small, depending on the distribution, one may design the system based on $B_1 n_1$ for particle radius anywhere in the approximate range $R = 0.1\mu m$ and $R = 1.0\mu m$, since $B_1 n_1$ is roughly constant. Then, since $B_1 n_1$ increases rapidly below $R = 0.1\mu m$ (due mostly to the Cunningham slip factor), the agglomeration times τ_A for the smaller particles become smaller (inversely proportional to $B_1 n_1$), while the self-repulsion time τ_R remains unaffected. In other words, if the agglomeration works well for particles of radius, say, $R = 0.1\mu m$, it will work even better for smaller particles. As Zebel says (Ref. 5.6, p 35): ". . . small particles are very rapidly 'eaten up' by large ones."

5.4 Application to Typical Size Distributions

We may apply the above theory to some sample actual size distributions, in order to see how these distributions affect the operation of the system (τ_A, τ_R, and V). We have chosen the first 7 distributions from Table 2.1 of Sec. 2. (the remaining distributions are similar to one of the 7 chosen). In Table 5.2 we have labelled the distributions as #1, #2, etc., labelling the columns across the top. The horizontal entries denote the following:

$D_{m/2}$ = mass median diameter

σ_g = geometric standard deviation

D_g = geometric-mean diameter (count median)

$\overline{D}$ = count-mean diameter

$\overline{D^3}/\overline{D^2}$ = ratio of count-mean-cube diameter to count-mean-square diameter

F_2 = fraction of large particles

$F_2/\overline{D}$ = used in formula for $(\tau_R)_{min}$

$\overline{D^3}/\overline{D^2}/F_2$ = used in formulas for $\tau_A \mathcal{M}$ and $\mathcal{M}_{max}$

$\mathcal{M}_{max}$ = maximum mass loading

$\tau_A \mathcal{M}$ = $\mathcal{M}$ x agglomeration time

$\tau_R \mathcal{M}$ = $\mathcal{M}$ x repulsion time

$(\tau_A)_{min}$ = minimum agglomeration time ($\mathcal{M} = \mathcal{M}_{max}$)

$(\tau_R)_{min}$ = minimum repulsion time ($\mathcal{M} = \mathcal{M}_{max}$)

$(\tau_R)_{min}/(\tau_A)_{min}$ = ratio of minimum times

V_A = V(volts) to mix particles, evaluated with $t = (\tau_A)_{min}$

V_R = V(volts) to mix particles, evaluated with $t = (\tau_R)_{min}$

We see that $(\tau_A)_{min}$ = 3.313 sec is a reasonable value (for the time of residence in the agglomerator section such that significant agglomeration occurs) and is the same for all distributions. The voltages V_R required to bring the particles together, that is, to mix them before they disperse are, except for Case #4, under about 23 kilovolts (a reasonable maximum voltage) for all distributions. For Cases #3, #4, #6, and #7, $(\tau_R)_{min}$ is less than $(\tau_A)_{min}$. This means that once the particles are mixed, there will be some agglomeration of the large particles amongst themselves. This should not be serious for Cases #3 and #6.

47

Table 5.2 Effects of Distribution
(Distributions from Table 2.1)

Distribution ⟶	#1	#2	#3	#4	#5	#6	#7
$D_{m/2}$ (μm)	1.8	2.3	4.0	0.34	2.7	$D_g = 0.9$	15.9
σ_g	2.2	3.5	1.7	5.4	2.4	~3	1.59
D_g (μm)	0.2788	0.02075	1.7187	6.701×10^{-5}	0.2709	0.9	8.341
$\overline{D}$ (μm)	0.3804	0.04548	1.9785	2.778×10^{-4}	0.3974	1.646	9.288
$\left(\overline{D^3}/\overline{D^2}\right)$($\mu$m)	1.319	1.0495	3.475	0.0820	1.8406	18.38	14.28
F_2	0.6633	0.03525	1.00 $F_1 = 2.527$ $\times 10^{-5}$	7.91×10^{-6}	0.6356	0.9149	1.00 $F_1 = 4.41$ $\times 10^{-}$
$\dfrac{F_2}{\overline{D}(\mu m)}$	1.7437	0.7751	0.5054	0.02847	1.5994	0.5558	0.10767
$\dfrac{1}{F_2}\dfrac{\overline{D^3}}{\overline{D^2}}$ (μm)	1.989	29.77	3.475	10367.	2.896	20.09	14.28
$\mathcal{M}_{max}$ (g/cm^3)	3.845×10^{-6}	5.755×10^{-5}	6.717×10^{-6}	0.02004	5.598×10^{-6}	3.883×10^{-5}	2.760×10
$\tau_A \mathcal{M}$ (sec-g/cm^3)	1.274×10^{-5}	1.907×10^{-4}	2.226×10^{-5}	0.0664	1.855×10^{-5}	1.287×10^{-4}	9.146×10
$\tau_R \mathcal{M}$ (sec-g/cm^3)	3.223×10^{-5}	2.145×10^{-4}	1.633×10^{-5}	2.744×10^{-3}	4.305×10^{-5}	1.0379×10^{-4}	1.429×10
$\left(\tau_A\right)_{min}$ (sec)	3.313	3.313	3.313	3.313	3.313	3.313	3.313
$\left(\tau_R\right)_{min}$ (sec)	8.384	3.727	2.430	0.1368	7.690	2.672	0.5172
$\dfrac{\left(\tau_R\right)_{min}}{\left(\tau_A\right)_{min}}$	2.530	1.125	0.7335	0.04128	2.321	0.8065	0.1561
V_A (volts)	21506	26319	11485	27139	21309	12718	3668
V_R (volts)	8498	23396	15659	657243	9180	15769	23495

Case #4 seems to be highly singular. For example:

(1) D_g is less than one Angstrom unit

(2) The fraction of large particles (F_2) is excessively small, less than 10^{-5}.

One may suspect that the size-distribution for Case #4 is poorly represented by a log-normal distribution; therefore, the small ratio (0.04) of repulsion-to-agglomeration times, and the excessive voltage (657 kilovolts) to bring particles together, may be unrealistic for this case.

In summary, of the 7 cases studied, all except #4 and #7 appear to be reasonably amenable to agglomeration; these exceptional cases might also turn out to be amenable if their distributions could be more accurately characterized.

6. EVALUATION

6.1 Brief Summary

The filtration enhancement system considered here - which consists of charger and agglomerator sections (Figs. 2.1 and 2.2) - and the scientific areas requiring investigation, have been discussed in detail in Section 2. The basic objective is to agglomerate fine particles onto larger particles, hence improving prefilter efficiency. Sections 3-5 contain the initial results obtained on each of the areas of investigation, which can be summarized briefly as follows.

Results on the ionization distribution due to the charger section ^{85}Kr beta source are presented in Section 3. The beta source (Fig. 3.1) was fabricated, filled with 0.1 atm ^{85}Kr gas, and the induced ionization around the source measured in a geometry (Fig. 3.3) similar to the charger section (neglecting the collimators). Results for the specific ionization are given in Fig. 3.4. Also given in that figure are analytical results obtained neglecting all scattering effects. The reasonably good agreement suggests that for calculations where only the energy deposition is of interest (as here), rather than the electron distribution function, this is a good assumption. Based on these results a source strength of about 500 Ci ^{85}Kr was selected as a basis for further consideration, leading to an ion pair production rate near $10^{11}/(cm^3\text{-sec})$ at about 10 cm radially from the source.

The ion density distribution in the charger was investigated in Section 4, with approximate results given in Figs. 4.2 and 4.3. It is clear from these figures that regions of well-separated positive and negative ion distributions can be maintained near the oppositely charged plates (as in Fig. 2.2) with applied potentials of ≤ 20 kV. Thus, the air to be filtered is separated into two streams, one passing through a region of positive ions, the other through a region of negative ions. The charging process for the particulates, and the subsequent agglomeration of the oppositely charged particulates in the presence of the reversed electric fields (Fig. 2.2), are considered in Section 5.

The operating feasibility of induced agglomeration has been assessed on the basis of theoretically derived time-scales for charging, agglomeration, and space-charge repulsion. For logical choices of the parameters, we obtain reasonable agglomeration times (residence time in the agglomeration section such that significant agglomeration occurs, and therefore successful operation) of the order of seconds. In the agglomeration process, the small particles are consumed by the larger particles. With plate voltages on the order of 20 kV the particles can be oppositely charged in the two halves of the gas stream, and then the oppositely-charged clouds of particles can be brought together (mixed) in the agglomerator section - in a time shorter than that in which they would "explode" or disperse under their space-charge repulsion forces. Thus, dispersion is avoided, as well as the self-agglomeration of the large charged particles with one another (which takes place in the same order of time). The dispersal time, and therefore the voltage required, depends on the particle size distribution, but the agglomeration time does not. We have considered 0.1-μm-radius particles, and have argued that (a) smaller particles than these would be consumed even faster by the large particles, and that (b) particles with radii in the range 0.1μm to 1.0μm would be agglomerated onto the "supermicron" (above 1μm) particles about equally rapidly. Thus, it is expected that the size distribution would shift significantly toward the supermicron sizes, which is the desired goal.

As a consequence, we believe that the radiation induced particulate agglomeration system considered here could, in fact, lead to significant enhancement of the prefilter efficiency, and hence overall improvements in economy in operation of nuclear facility filtration systems.

6.2 Comparison of Results with Some Related Work

Heinsohn et al. (Ref. 2.1) have carried out an investigation of possible use of ^{60}Co gamma radiation for production of ionization in a particulate charging system. Their objective was to remove the particles, after being charged, by electrostatic precipitation - quite a different principle from the agglomeration technique investigated here. Yet, some of their results on ionization are quite useful for comparison. Their experimental system used two 75 Ci sources of ^{60}Co; the ionization was produced by Compton and photoelectric electrons ejected in their experimental housing by the ~1 MeV ^{60}Co gamma rays. Their maximum measured specific ionization was about

$$4.8 \times 10^9 [\text{ions}/(\text{cm}^3\text{-sec})]/(2 \times 75 \text{ Ci}) \approx 3 \times 10^7 \text{ ions}/(\text{cm}^3\text{-sec-Ci} \gamma\text{'s}) \quad (6.1)$$

Note that this is several times less than the specific activity in the 10-20 cm region of Fig. 3.4. Furthermore, the radiation hazard external to the apparatus that is associated with ^{85}Kr, when measured per curie, is far less than that due to ^{60}Co. The ^{85}Kr gamma ray (~0.5MeV) is emitted in only 0.4% of the decays, and the efficiency of conversion of the 99.6% emitted beta energy into bremsstrahlung (≤ 670 keV, avg~300 keV) is less than 1%. Thus, on a radiation hazard basis ^{85}Kr is less than about 1% of a similar source strength ^{60}Co source. We concur with Heinsohn et al. (Ref. 2.1), who note in their conclusion that since it is, in fact, electrons which produce the ionization, they can more easily be provided by beta than gamma radiation. We note, for example, that the 500 Ci ^{85}Kr beta source found here to provide the ~10^{11} ions/(cm^3-sec) needed ionization rate, is equivalent to only 5 Ci of external (to the apparatus) electromagnetic radiation

51

(γ's and bremsstrahlung). It is also of interest to note that the resulting ion densities are similar to those typically found in electrostatic precipitators (Refs. 5.2 and 6.1), but that our method of production of the ionization requires much less power.

Regarding electrically-induced agglomeration studies by Melcher and Sachar (Ref. 6.2), they did not consider radii below one micrometer, and hence did not consider fine particles. They artificially chose two groups, a 1.0-μm-radius group to represent all the "small" particles, and a 10.0-μm-radius group to represent all the "large" particles in a distribution; whereas we consider a series of entire log-normal distributions, all based on actual nuclear facility particle distributions. (Our small-particle fraction as a function of particle radius is assumed to be given by the integral over the log-normal distribution, from zero radius to the radius of interest. This is based on the analytical fall-off behavior of the log-normal distribution at small radii, and may be considered a natural way of characterizing the small-particle fraction.) In Ref. 6.2 it was assumed that the "small" and "large" oppositely-charged particles were somehow instantaneously charged and mixed. This seems somewhat artificial as opposed to our method of charging and of bringing the particles together, under controlled conditions. Also, in Ref. 6.2 a special ratio of dust loading distributed between the "small" and "large" particles is postulated in order to achieve efficient operation; it is difficult to see how this ratio can be controlled in practice. In our method, the total dust loading is the (more practical) parameter affecting the rate of agglomeration. The values of dust loading assumed in Table 5.2 leading to successful operation are typically found in industrial electrostatic precipitators (Ref. 6.1).

7. RECOMMENDATIONS

Based on the above evaluation, we believe that experimental and supporting analytical work should be carried out to make preliminary tests of the charger section, as the first part of Phase II. In particular, the following tasks can be defined:

1) Design experimental model charger section and fabricate.

2) Measure ion density distribution in charger section (Langmuir probe or similar instrument).

3) Modify theory based on Phase I results and apply to obtain better estimates of particulate charging and agglomeration.

4) Measure actual state of charging on simple (0.3μm monodisperse) particulates (mobility analyzer or similar instrument).

5) Analyze results, write report and suggest agglomeration studies if charging results justify it.

It is expected that item 4) would be carried out by use of laboratory facilities at the Harvard School of Public Health, under the overall supervision of Dr. Melvin W. First. It is intended that the minimum source intensity will be used that is sufficient to demonstrate the charging principles. Maximum use will be made, in the experiments, of lower than actual flow rates, since the flow rate is a parameter that occurs in the theory. Once the system concept has been verified for low source strengths and flow rates, results can be predicted with confidence for realistic system parameters.

REFERENCES

2.1 Heinsohn, R. J., Levine, S. H., Fjeld, R. A. and Malamud, G. W., "Radiation Charging: A Novel Way to Electrically Charge Fine Particles," 409-46 in Symposium on Electrostatic Precipitators for the Control of Fine Particles, EPA-650/2-75-016, C. E. Feazel, Editor (1975).

2.2 Nelson, G. O., Miller, B. H., Richards, C. P., and Bierman, A. H., Enhanced Filtration, July-Sept. 1976 Progress Report, Lawrence Livermore Laboratory Report No. UCID-16949-76-3 (March, 1977).

3.1 Varma, M. N. and Baum, J. W., New "wall-less" ionization chamber for air dose measurement, Rev. Sci. Instru. $\underline{47}$ 112-114 (1976).

3.2 Hogan, O. H., Zigman, P. E., and Machin, J. L., Beta Spectra II. Spectra of Individual Negatron Emitters, USNRDL-TR-802, (Dec. 1964). AD 455961.

3.3 Berger, M. J. and Seltzer, S. M., Tables of Energy Losses and Ranges of Electrons and Positrons, NASA SP-3012 (1964).

5.1 Dennis, R., editor, Handbook on Aerosols, ERDA Report TID-26608 (1976).

5.2 White, H. J., Industrial Electrostatic Precipitation, Addison-Wesley, Reading, Mass. (1963).

5.3 Parker, L. W., "Field Charging Theory for Electrostatic Precipitation of Ultrafine Particles," 68th APCA Annual Meeting, Boston (1975); also, Liu, B. Y. H. and Yeh, H-C, J. Appl. Phys. $\underline{39}$ 1396 (1968).

5.4 Davies, C. N., Air Filtration, Academic Press, New York (1973).

5.5 Parker, L. W., in Precipitation Scavenging (1974), R. G. Semonin and R. W. Beadle, editors, ERDA Symposium Series No. 41 (CONF-741003), pp. 276-298 (1977).

5.6 Zebel, G., in Aerosol Science, C. N. Davies, editor, Academic Press, New York, pp. 31-58 (1966).

6.1 Oglesby, R. and Nichols, G. B., Southem Research Institute Report, A Manual of Electrostatic Precipitator Technology, Part I, Fundamentals, PB-196380 (1970).

6.2 Melcher, J. R. and Sachar, K. S., Electrical Induction of Particulate Agglomeration, MIT Report PB-205188 (1971).